Type Ia Supernovae: Explosions and Progenitors

Wolfgang Eitel Kerzendorf

A thesis submitted for the degree of

Doctor of Philosophy

of The Australian National University

THE AUSTRALIAN NATIONAL UNIVERSITY

Research School of Astronomy and Astrophysics
The Australian National University
Canberra ACT 0200
Australia

July 2011

Fancy schmancy italic text for a dedication.

Disclaimer

I hereby declare that the work in this thesis is that of the candidate alone, except where indicated below or in the text of the thesis.

Wolfgang E. Kerzendorf

12th July 2011

Acknowledgments

Lorem ipsum dolor sit amet, consectetuer adipiscing elit. Donec tincidunt semper neque. Cum sociis natoque penatibus et magnis dis parturient montes, nascetur ridiculus mus. Donec cursus velit ut felis. Quisque tellus. Curabitur in leo. Suspendisse volutpat. Nunc sodales sagittis magna. In vehicula viverra elit. Donec dapibus cursus mauris. Maecenas volutpat, sapien eu dictum molestie, mi lectus tristique augue, eu lobortis tellus nisi nec urna. Phasellus at est nec odio ultricies consequat. Nam eu urna.

Duis tempus imperdiet nunc. Integer vitae lorem. Sed id pede eu turpis rhoncus semper. Curabitur ante leo, facilisis vitae, interdum mollis, fermentum et, ipsum. Phasellus scelerisque, arcu et varius venenatis, lacus magna semper mauris, et aliquet augue nulla hendrerit libero. Suspendisse nec turpis et nisl congue posuere. Mauris sagittis ipsum nec lectus. Vestibulum nisl. Quisque ante. Nam accumsan, metus eu lobortis laoreet, massa velit elementum urna, ac tristique eros justo sit amet mauris. Vestibulum at arcu hendrerit massa placerat tristique. In magna velit, vestibulum eget, viverra ut, facilisis id, lectus. Cras justo lorem, varius non, tristique sit amet, lobortis nec, neque. Aenean cursus congue metus. Vestibulum id magna.

Abstract

Lorem ipsum dolor sit amet, consectetuer adipiscing elit. Donec tincidunt semper neque. Cum sociis natoque penatibus et magnis dis parturient montes, nascetur ridiculus mus. Donec cursus velit ut felis. Quisque tellus. Curabitur in leo. Suspendisse volutpat. Nunc sodales sagittis magna. In vehicula viverra elit. Donec dapibus cursus mauris. Maecenas volutpat, sapien eu dictum molestie, mi lectus tristique augue, eu lobortis tellus nisi nec urna. Phasellus at est nec odio ultricies consequat. Nam eu urna.

Duis tempus imperdiet nunc. Integer vitae lorem. Sed id pede eu turpis rhoncus semper. Curabitur ante leo, facilisis vitae, interdum mollis, fermentum et, ipsum. Phasellus scelerisque, arcu et varius venenatis, lacus magna semper mauris, et aliquet augue nulla hendrerit libero. Suspendisse nec turpis et nisl congue posuere. Mauris sagittis ipsum nec lectus. Vestibulum nisl. Quisque ante. Nam accumsan, metus eu lobortis laoreet, massa velit elementum urna, ac tristique eros justo sit amet mauris. Vestibulum at arcu hendrerit massa placerat tristique. In magna velit, vestibulum eget, viverra ut, facilisis id, lectus. Cras justo lorem, varius non, tristique sit amet, lobortis nec, neque. Aenean cursus congue metus. Vestibulum id magna.

CONTENTS

LIST OF FIGURES

LIST OF TABLES

CHAPTER 1

INTRODUCTION

FOR millenia mankind has watched and studied the nightsky. Apart from planets and comets it appeared an immuatble canvas on which the stars rested. It comes as no surprise that for ancient civilizations supernovae (which were very rare events, occuring only every few centuries) were interpreted as important omens as they broke the paradigm of the unchanging nightskies. As these events are so rare their origin remained a mystery until the middle of the last century. **?** suggested that "the phenomenon of a super-nova represents the transition of an ordinary star into a body of considerably smaller mass". For the last 85 years the "supernova-branch" in astronomy has been developing. There have been many advances, but there are still many unknowns. This work addresses two subfields of supernovae: The unsolved progenitor problem for Type Ia Supernovae as well as quantifying the nucleosynthetic yield and energies of Type Ia supernovae.

1.1. Ancient Supernovae

One of the earliest recorded supernovae is SN185. It first appeared in December of 185 and was visible (however fading) till the August of 187. The main record is the *Houhanshu* (**?**) which had a described it to be close to α *cen*. Follow-up in modern times have revealed a supernova remnant in a distance of roughly 1 kpc near the α *cen* (**?**). SN185 is often named as the oldest written record of a supernova, this is however sometimes contested as it is still not completely clear if the so called "guest star" was a comet or a supernovae.

The oldest undisputed record of a supernova is SN1006, which also coincides with the brightest ever recorded supernova. It was observed worldwide by asian, arabic and european astronomers. **?** gives a good summary of the observations and interpretation given by these ancient observers. Ali ibn Ridwan was an Egyption astronomer who recorded the appearance of SN1006. He wrote in a comment on Ptolemy's *Tetrabiblos*: "*I will now describe for you a spectactle that I saw at the beginning of my education. This spectacle appeared in the zodiacal sign Scorpio in opposition to the sun, at which time the sun was in the 15th degree of Taurus and the spectacle in the 15th degree of Scorpio. It was a large spectacle, round in shape and its size 2.5 or 3 times the magnitude of Venus. Its light illuminated the horizon* *and twinkled very much. The magnitude of its brightness was a little more than a quarter of the brightness of the moon. It continued to appear and it moved in that zodiacal sing Virgo, in setile to it, and ceased (appearing) all of a sudden. This apparition was also observed at the time by (other) scholars just as I have recorded it.* "

SN1006 was later found to be a Type Ia supernova and is of significance importance in this work (see chapter **??**).

? detected a pulsar in the center of SN1054. This was the first time that the stellar remnant of a supernova was found. SN1054, like SN1006, was observed by many astronomers. One of the records is a muriel in the Chaco Canyon (see Figure **??**) and was determined to have been produced around the time of the SN1054 explosion. It is still debated if SN1054 was the inspiration of the painting or the inspiration came from the passing of Hailey's comet in 1066.

SN1181 is a Galactic supernovae that has been mentioned in eight different texts by Chinese and Japanese astronomers. 3C58, a pulsar found in SN1181, is suggested as the neutron star remnant of this stellar explosion.

Figure 1.1 example caption

The supernova of 1572 has been reported by many astronomers. The most famous record, however, stems from the danish astronomer Tycho Brahe (**?**). The supernova was observed from November 1572 and monitored till March 1574 when it faded away from visibility. Figure **??** shows the original chart produced by Tycho Brahe which shows the supernova in the constellation of Cassiopeia. Nearly 400 years later **?** discovered the radio emissions from the remnant of the SN1572. SN1572 is discussed in detail in chapters **??** & **??**.

Thirtytwo years after the discovery of SN1572 **?** and others observed SN1604. The super-

nova remained visible for about 18 month. It will be discussed in this work in chapter **??**.
???? <—- This is the conclusion chapter ????

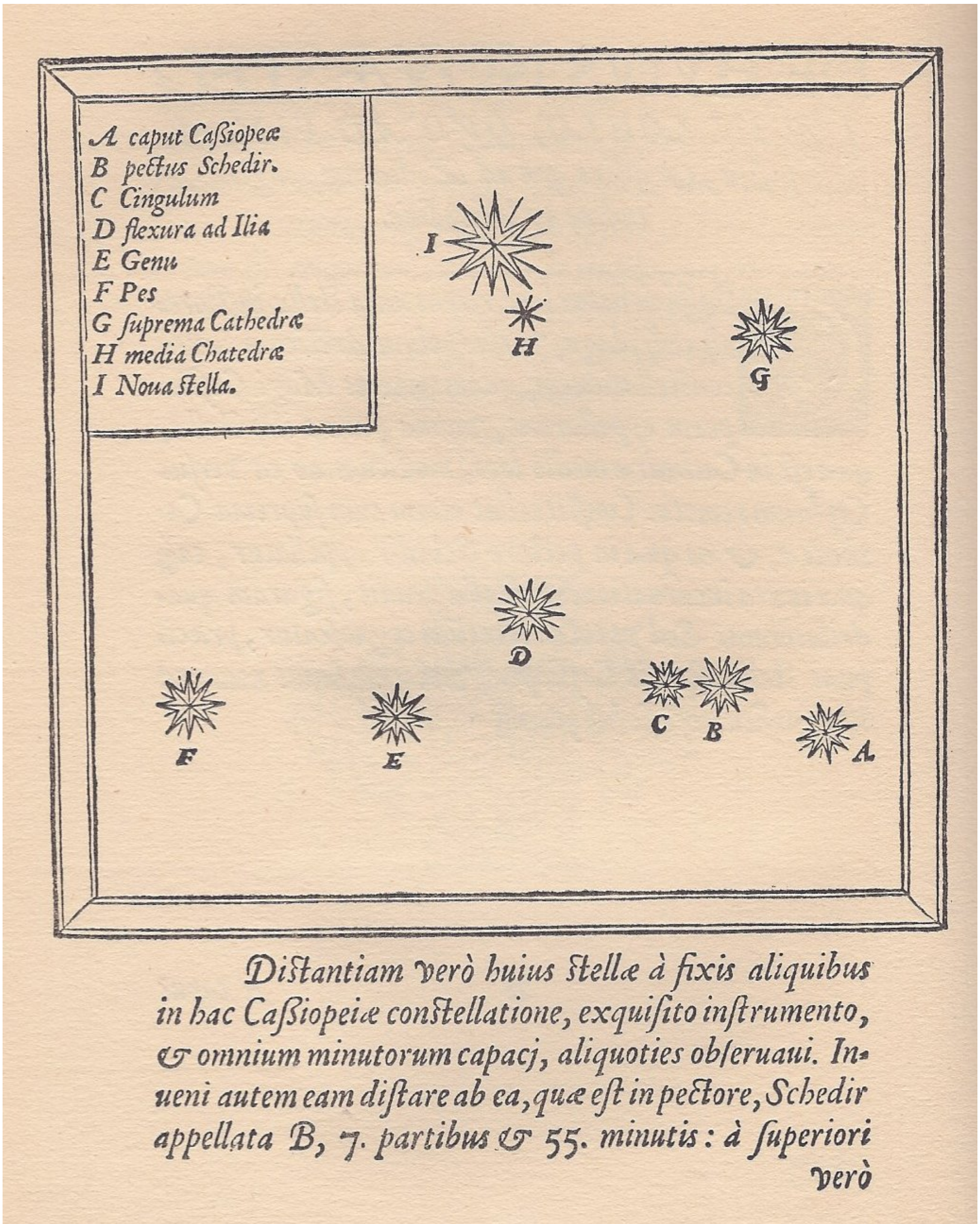

Figure 1.2 *"I have indeed measured the distance of this star from some of the fixed stars in the constellation of Cassiopeia several times with an exquisit (optical) instrument, which is capable of all the fine details of measurement. I have further detected that it (the new star) is located 7 degrees and 55 minutes from the star at the breast of the Schedir designated by B."* translation kindly provided by Leonhard Kretzenbacher

All of the ancient supernovae were observed only by the naked eye. Even in an era with

10-meter telescopes the records of these explosions remain useful.

1.2. Modern day supernova observations

The era of modern day supernova observations started with the discovery of SN1885. SN1885 (S Andromedae) was first spotted by Isaac Ward in Belfast in August of 1885 (**?**) and was visible till February 1886. More than 50 years later **?** coined the term supernova and established the difference between common novae and supernovae. **?** also suggested that these luminous events are caused by the death of stars.

In order to understand the phenomenon of the supernova better, Zwicky began a supernova search with the 18-inch Schmidt telescope. Zwicky found several supernovae which in turn inspired Minkowski to classify these supernovae by their spectra **?**. He categorized the 14 known objects into two categories. Those without hydrogen he called 'Type I', those with hydrogen he called 'Type II' (see section **??** for a more detailed description).

With the advent of affordable computing in the 1960s the first computer controlled telescopes were build. The 24-inch telecope was built by the Northwestern University and was deployed in Corralitos Observatory in New Mexico. This search resulted in 14 supernovae.

The 1990's can be described as the decade of the supernova surveys. The Leuschner Observatory Supernova Survey began in 1992 followed shortly by the Berkeley Automatic Imaging Telescope (BAIT). These searches resulted in 15 supernovae by 1994 (**?**). One of the most well known discoveries is SN 1994D. This supernovae was observed with the Hubble Space Telescope and resulted in an image that is widely used today (see Figure **??**).

These successful programmes were succeeded by the Lick Observatory Supernova Search (LOSS) using the Katzman Automatic Imaging Telescope (KAIT). By the year 2000 it had found 96 supernovae (**?**).

In addition to the search in the optical new high-energy instruments like BATSE surveyed the sky in gamma-rays. **?** that GRBs due to their isotropic distribution are events at cosmlogical distances rather than coming from our own Galaxy.

It was followed by the SWIFT telescope which provides, in addition to the gamma-ray-detector, an X-Ray telescope and UV/Optical telescope. It has been very successful at finding GRBs and providing targets for follow-up.

After the turn of the millenium and following the discovery of the accelerated expansion of the universe a variety of groups searched for supernovae and other transients. Some of the main contributors are the ESSENCE-collaboration,

1.3. Observational Properties of Supernovae

1.3.1. Supernova classification

The classification of supernovae started in the 1941 when Minkowski realized that there seem to be two main types (**?**). Those containing a hydrogen line (6563 Å) he called Type II supernovae and those showing no hydrogen he called Type I supernovae.

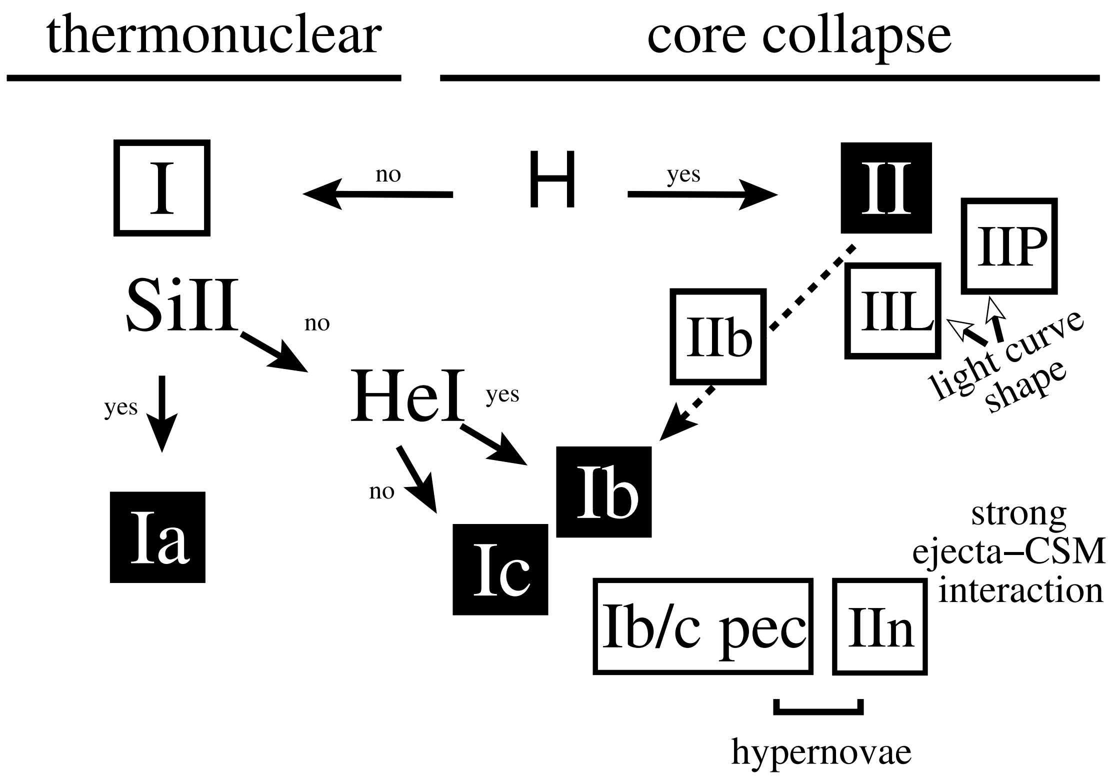

Figure 1.3

This basic classification has remained to this day, however the two main classes branched into several subclasses. During the 1980s the community discovered that most SNe Ia showed a broad Si II line at 6130 Å. There was, however, a distinct subclass of objects that lacked this feature. These Silicon-less objects were then subclassed further into objects that showed helium – now known as Type Ib – and those that did not were called Type Ic (**??**). The classical Type I supernova was renamed to Type Ia (see Figure **??**).

This classification only uses static spectral features. In recent years, however, there has been a push towards also using the lightcurve and spectral evolution as classification parameters. **?** provide an overview of this subclassing of SNe Ia and suggest that there are two distinct subclasses of SNe Ia. As a parameter for this further partitioning they use the velocity measured from the Si II feature at 6130 Å. Those with a relatively fast decline in this radial velocity they call HVG (high velocity gradient) those with a slow decline rate are named LVG (low velocity gradient). Figure **??** shows the velocity gradient of 26 supernovae taken from **?**

Futhermore there seems to be also a split in the intrinsic luminosity of SNe Ia. The canonical objects for these distinct brightness classes are the overluminous 1991T **?** and the faint 1991bg. Faint supernovae are fast decliners both in velocity as well as luminosity **?**. The bright supernovae seem to occur in both the HVG and LVG group. I will discuss the physical implications of these two subtypes in section **??**.

In summary, although there are several different subclasses the SN Ia as a class itself is relatively homogenous when compared to the different SNe II.

SNe II span large ranges in observable parameters. We can divide the main class into

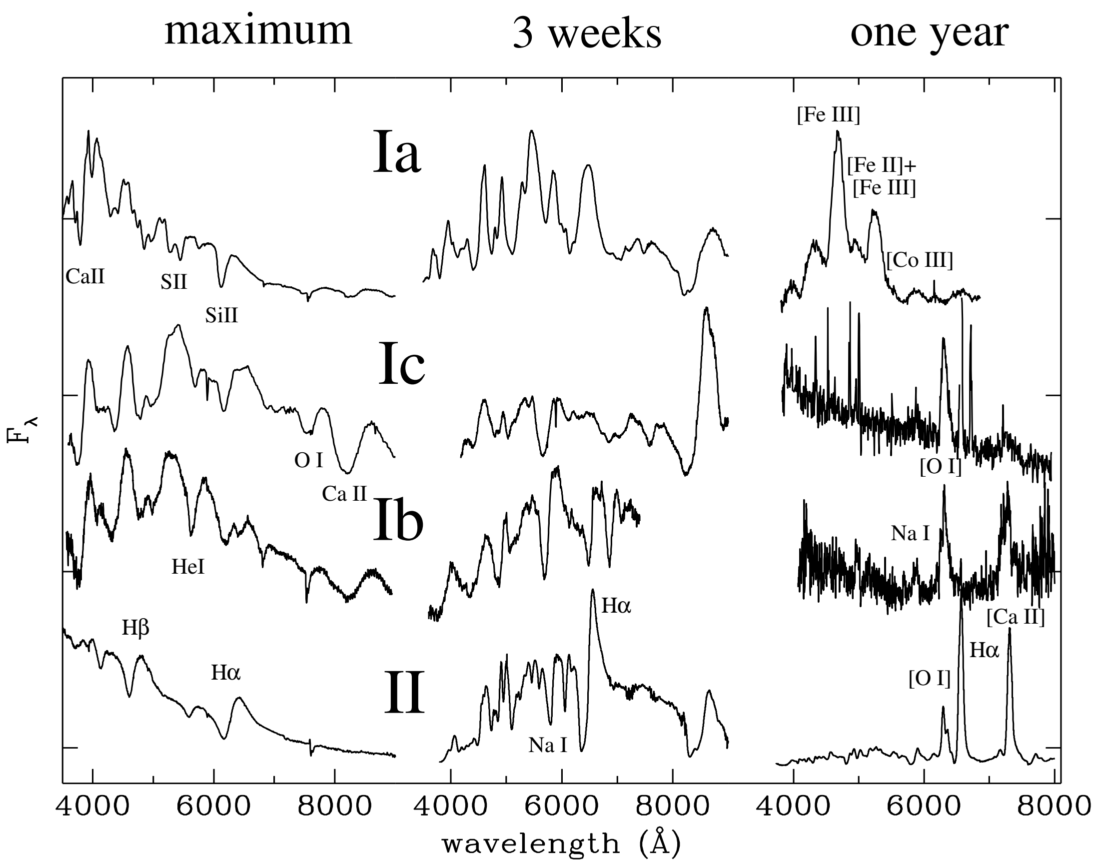

Figure 1.4 example caption

three main subclasses Type II Plateau **?** which have a relatively flat light curve after an initial maximum (see Figure **??**), in contrast the Type II Linear (SN IIL **?**) has a rapid linear decline after the maximum. The third subclass is the narrow-lined SN II(SN IIn) which is characterized by narrow emission lines, which are thought to come from interaction with the CSM. Unlike the SNe Iathere are numerous intermediate objects among these three basic classes and some peculiar objects.

For a more comprehensive review of the classification of supernovae the reader should consult **??**.

1.3.2. Supernova rates

The observed supernova frequency carries important information about the underlying progenitor population. In this section we will concentrate more on SNe Ia-rates but will mention SNe II and SNe Ib/c where applicable.

? was the first work that tried to measure the supernova rate. By monitoring a large number of fields monthly, they arrived at a supernova rate by merely dividing the number of supernova detection by the number of monitoring time and galaxies. This crude method resulted in a rate of one supernova per six centuries.

Over time many improvements were made to this first method. The rate was divided

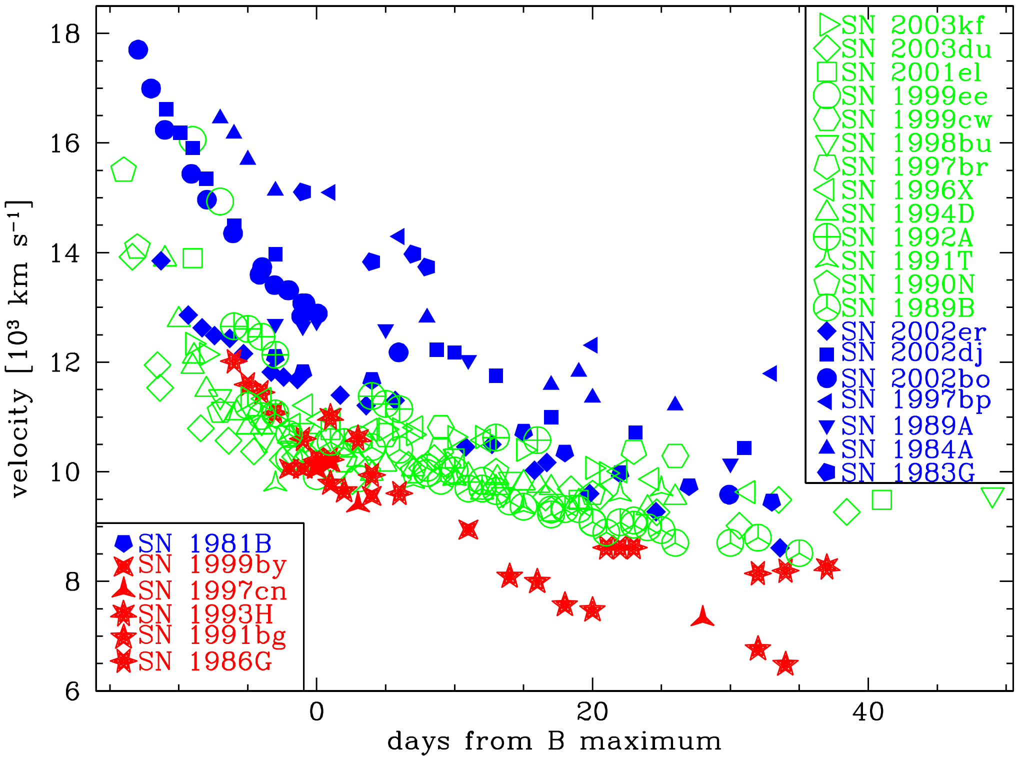

Figure 1.5 example caption

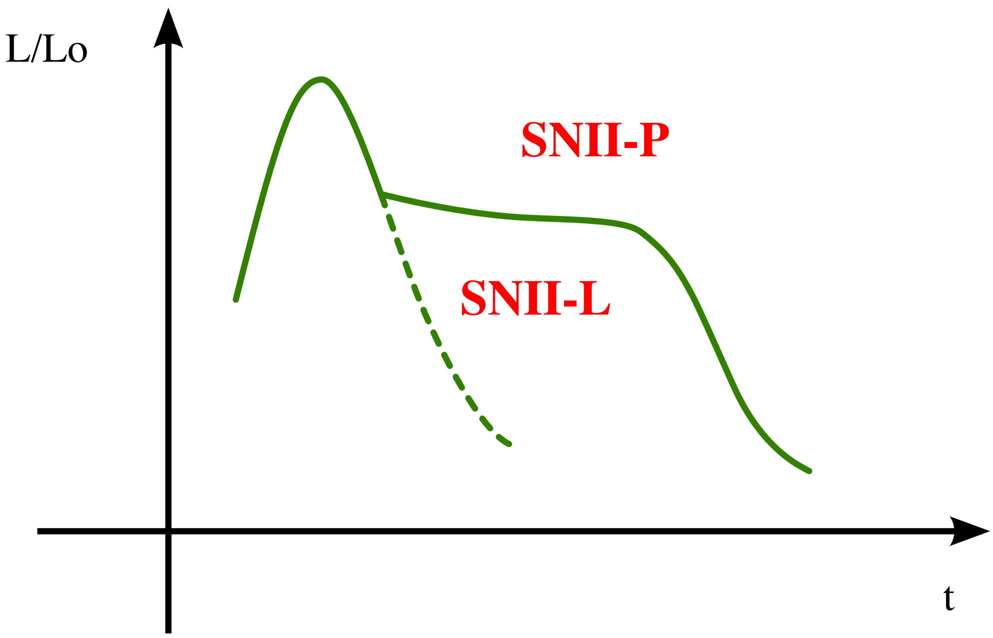

Figure 1.6 example caption

by galaxy morphological class as well as different supernova types. In addition, rates were then defined the supernova rate as number of events per century per $10^{10}\,L_\odot$ (e.g. **??**). In recent years, however, rate measurements is in relation to star formation rather than photometry (SN per century per $10^{10}\,M_\odot$). Therefore the community (e.g. **?**) have switched to the use of infrared photometry for the galaxy as it is thought to better represent star-formation rate then B-Band photometry (**?**).

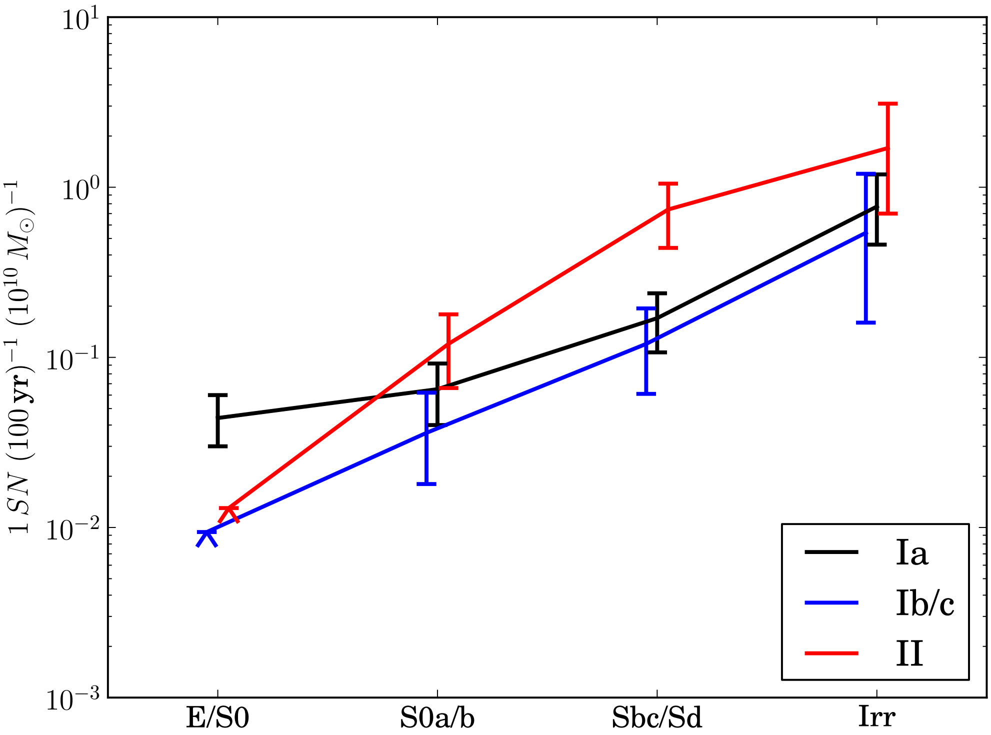

Figure 1.7 example caption

Figure **??** clearly shows that there is a strong connection between morphology and supernova rates. Both progenitor scenarios (single-degenerate and double-degenerate) suggest an "evolved" binary system. It is therefore puzzling that most supernovae occur in late-type spirals with a relative young stellar population. In addition, there is evidence that underluminous SNe Ia (e.g. SN 1991bg) are twice as common in late-type galaxies than in early-type galaxies (**?**). Furthermore it appears that radio-loud early-type galaxies have an enhanced rate of SNe Iaover radio-quiet galaxies (**?**).

All of these factors suggest that SNe Ia can originate from two distinct progenitor scenarios and/or different explosion mechanisms (**??**).

1.3.3. Light curves

Light curves were the first observables of supernovae. It contains

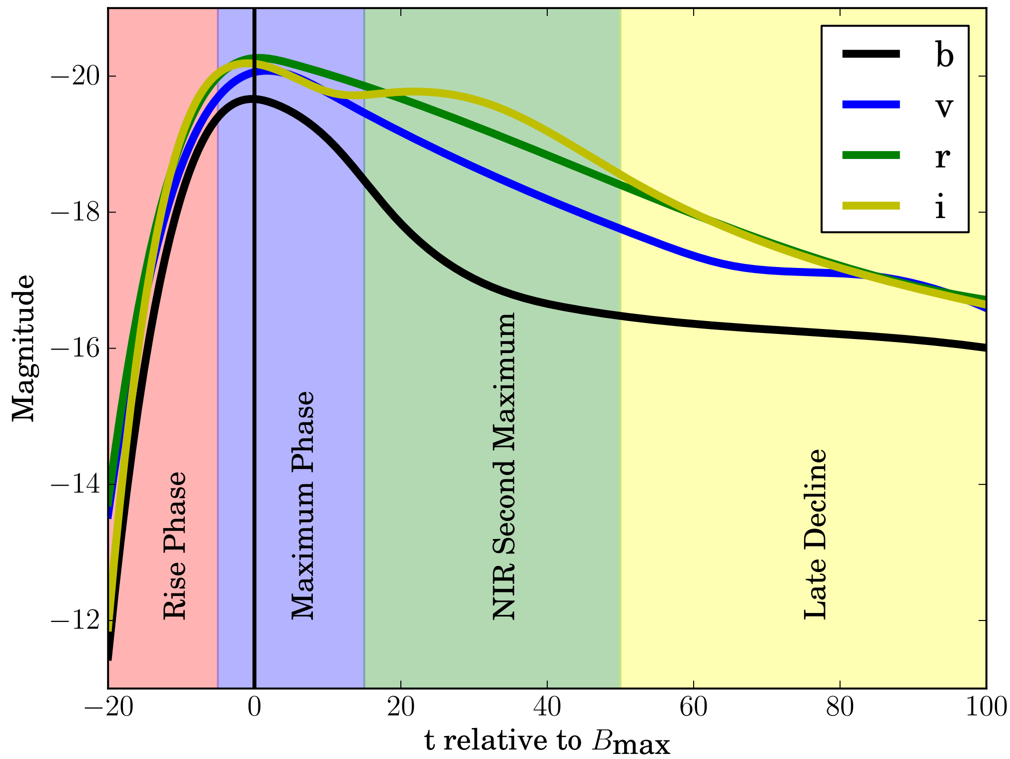

Figure 1.8 example caption

The light curve can be divided in four different phases (see Figure **??**). In the first phase the SNe Ia rises to the maximum brightness. Although only a small fraction of SNe Iahave been observed in that phase, one can determine the time of the explosion by approximating the very early phase of a SNe Iawith an expanding fireball. The luminosity of the fireball is

$$L \propto v^2(t + t_r)^2 T\,,$$

where v is the photospheric velocity, T is the temperature of the fireball, t is the time relative to the maximum and t_r is the rise time. A rise time of 19.5 days (**?**) seems to fit most SNe Ia.

The rise is very steep and the brightness increases by a factor of ≈ 1.5 per day until 10 days before maximum.

The SN Iareaches the maximum first in the NIRroughly 5 days before the maximum in the B-Band (**?**). During the pre-maximum phase the color stays fairly constant at B-V=0.1, but changes non-monotonically to B-V=1.1 30 days after maximum.

The SN Ia starts to fade but a second maximum is observed in the NIR(**?**) ??multiple citations. (**?**) has succesfully explained this by fluorescence of iron-peak elements in the NIR. See section **??**.

At roughly 600 days after maximum the light curve begins ???? 1991t had a foreground dust???

Arguably the most important use of light curves is their application in normalizing SNe Ia to standard candles (see Figure **??**). **?** plotted the magnitude at maximum in different filters against the decline of the B-Band magnitude after 15 days ($\Delta\, m_{15}(B)$). They found a strong linear relation with a very high correlation coefficient (> 0.9). Dust extinction in the host is one of the major systematic problems and remains so to this day.

? refined the method by using a linear estimation algorithm. This method would deliver a distance modulus by finding the offset between a template and the supernova lightcurve. They calibrated this method against a set of SNe Ia with known distances. Light curve fitting tools are to this day in active development (e.g. **??**).

In summary, ... see figure x

1.3.4. Spectra

Spectra are much more detailed measurements of Supernovae. They are however, observationally much more expensive.

Supernovae spectra can be divided in two phases: the photospheric phase and the nebular phase. In the photospheric phase, the spectrum can be very well approximated by a dense optically thick core which has a black-body radiating surface. Above this photosphere is an optically thin ejecta wind. Photons are usually not created in the optically thin ejecta. The ejecta rather reprocesses the radiation field coming from the photosphere. In the case of SNe Ia the core consists mainly of decaying ^{56}Ni which produces the energy for the radiating photosphere. For SNe II the core consists mainly of ionized hydrogen.

As the supernova expands the photosphere recedes further into the core and the optically thin layer grows larger and larger. Once sufficiently expanded the entire SN ejecta becomes optically thin. This phase is dominated by strong emission peaks and no continuum.

SNe Ia spectra

SNe Ia spectra span many different applications, but foremost they help us to understand the physical processes in the thermonuclear explosion. Shortly after the explosion the ejecta is in homologous expansion. The observed spectra are characterized by an underlying continuum - emitted from the photosphere – and absorption features from the ejecta material above the photosphere. As time passes the photosphere recedes into the remnant and deeper layers of the exploded white dwarf become spectroscopically visible. Synthetic modelling of spectra is an important component to understanding SNe Ia and will be discussed in detail in Chapter **??**.

This time-variability in the spectra is used to conduct tomography on SNe Ia(**?**).

Similar to light-curves the spectra have different phases. We will use the "normal′-SN IaSN 2003du to demonstrate the spectral evolution (**?**).

Pre-Maximum Phase In the pre-maximum phase the spectrum shows very high velocities (up to 18 000 km s^{-1}). There is a relatively well defined pseudo-continuum with strong P Cygni-profiles of IMEs and iron-group elements (see Figure **??**). These iron-group elements are primordial as the burning in the outer layers (visible at these early times) is incomplete and does not produce these elements.

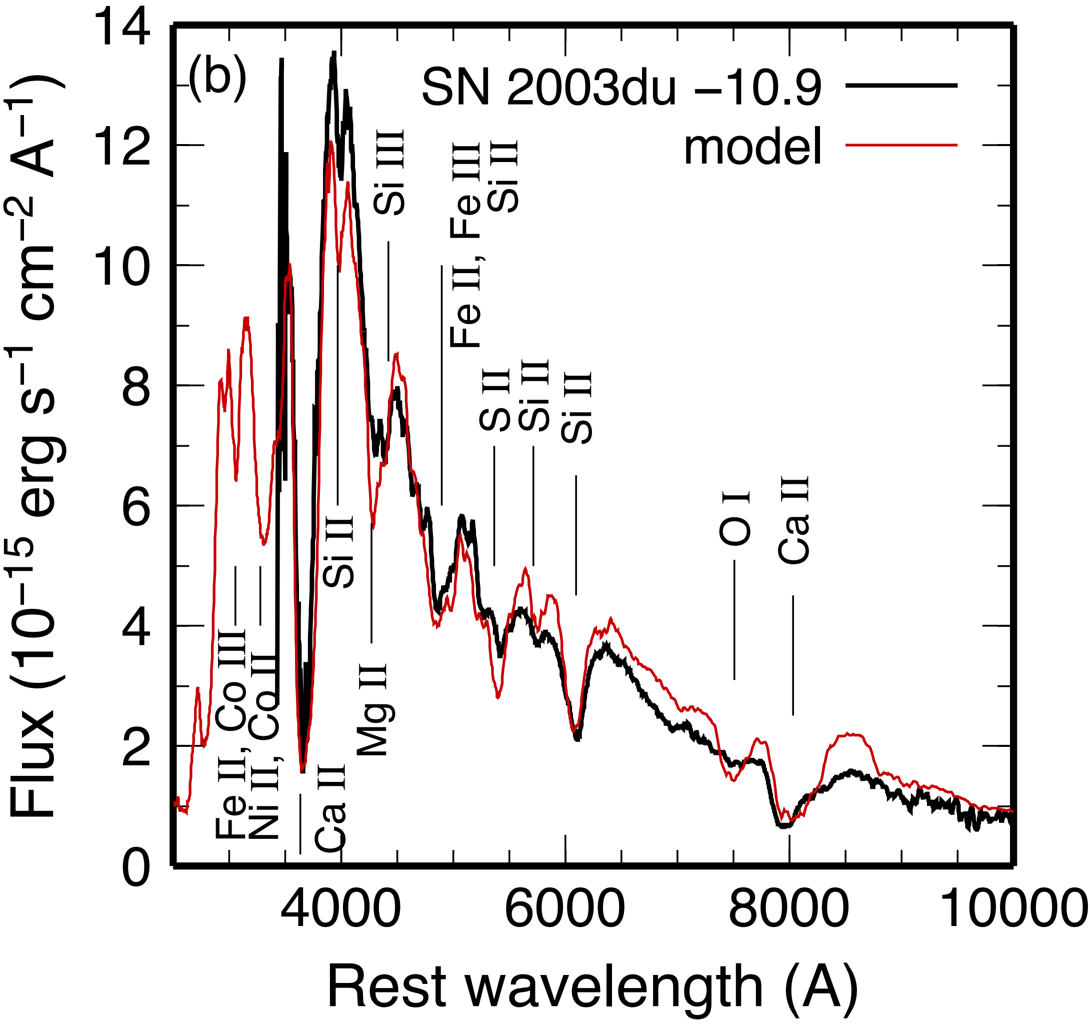

Figure 1.9 example caption

The Ca Roman2 line is very prominent in the blue and often shows extremely high velocities at early times (in SN 2003du v 25000 km s^{-1}). There have been multiple suggestion for the cause of this unusual velocity, including interaction with Calcium in the ISM or high-velocity ejecta blobs (**???????**). There is a strong Mg Roman2 feature at 4200 Å which is contaminated by several iron lines. Silicon and Sulphur both have strong features 5640 Å(S Roman2) and at 6355 Å(Si Roman2). The strong Silicon feature distinguishes SNe Iaagainst other supernovae in the Type I-group.

It is believed that in these early phases one should be able to see Carbon and Oxygen from the unburned outer layers. There is the C Roman2-feature at 6578 Åbut it is normally very weak (if visible at all). The Oxygen triple feature at 7774 Å is seldom very strong. ??? ask stephan ??

Maximum Phase As the supernova rises to the peak luminosity a large fraction of iron group elements (especially ^{56}Ni) is suppressing flux in the UV and reemitting it in the optical (see Figure **??**). The silicon lines become narrower (??only in 03du??) as the photosphere reaches material deeper in the remnant. The ratio of the Silicon lines Si Roman2 5972 Åand Si Roman2 6355 Åis a good indicator for temperature (**?**).

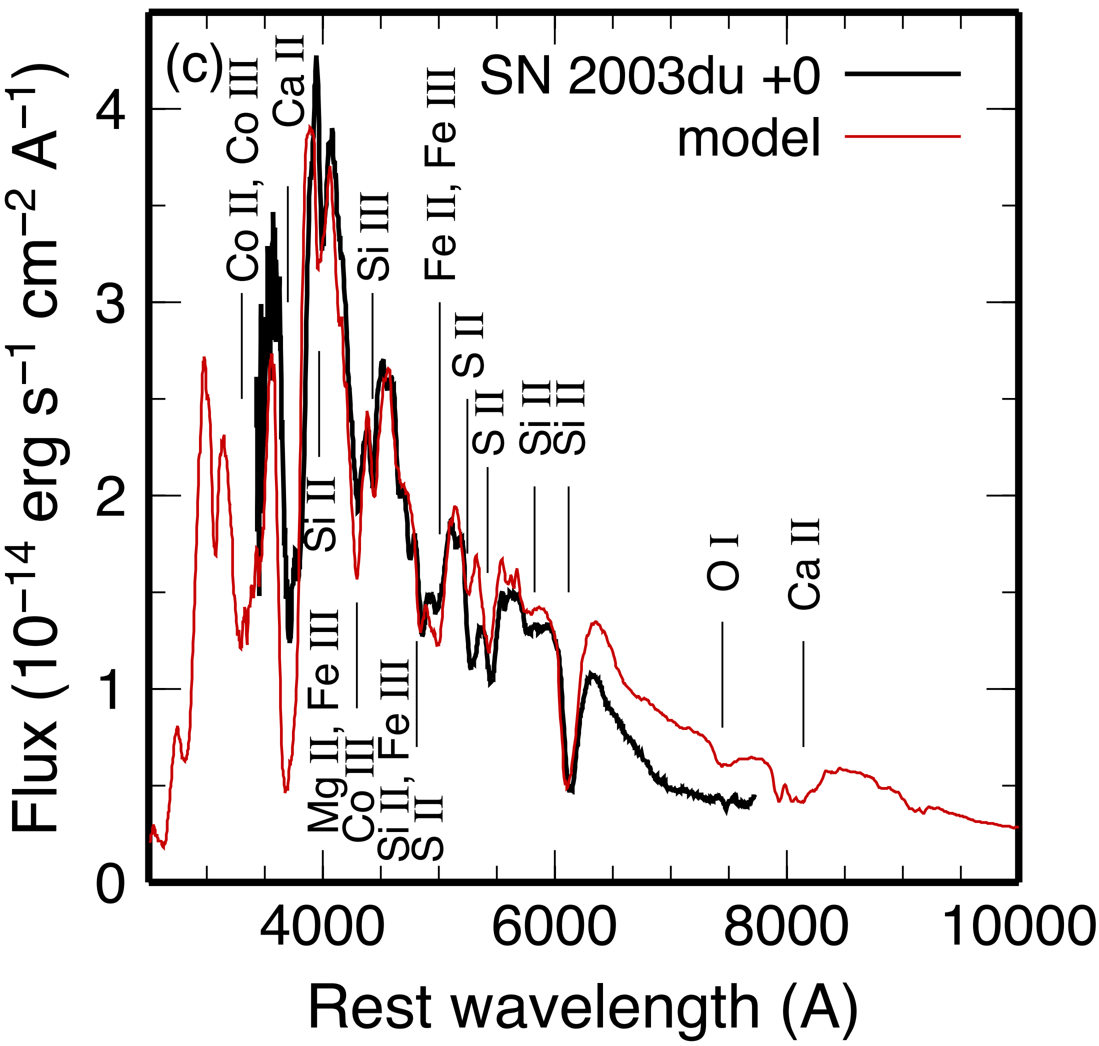

Figure 1.10 example caption

Post-Maximum phase The contribution from iron-group elements is still rising, while the photospheric velocity has decreased to less than 10000 km s^{-1}(see Figure **??**). The strong Calcium feature at 4000 Å is disappearing.

Nebular-Phase As the supernova fades, the photosphere disappears. At this stage the spectrum is now characterized by strong emission lines which are produced by the elements from the very core of the explosion (see Figure **??**). The velocity has fallen under 5000 km s^{-1}(??check??).

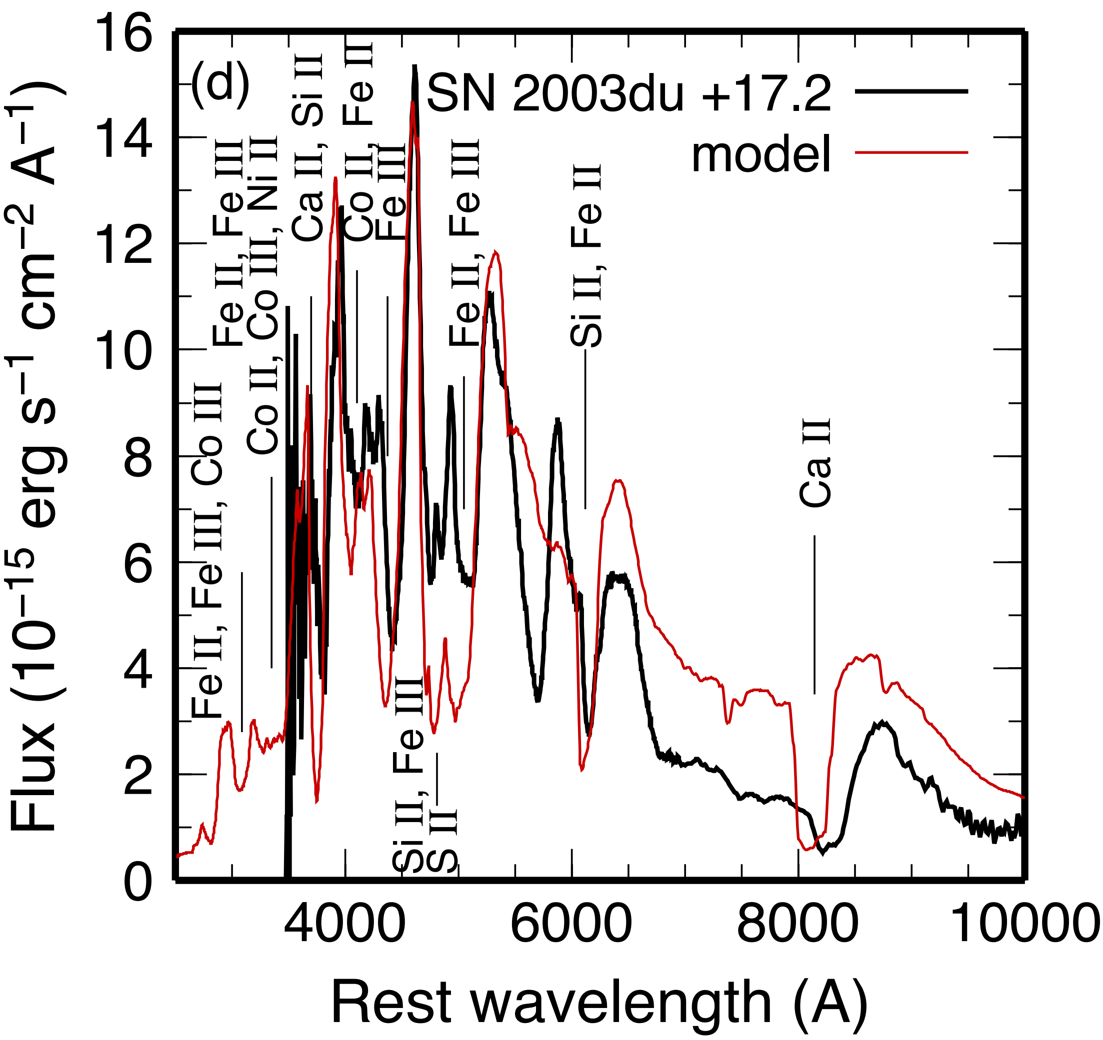

Figure 1.11 example caption

SNe II Spectra

SNe II show much more variation in their spectra for each object than SNe Ia . In this section we will only give a very general and brief overview over SNe II spectra and spectral evolution. Compared to SNe Ia the initial spectrum is a relatively undisturbed continuum (see **??**). The only strong lines visible are those of Hydrogen and Helium which are the elements present in the envelopes of the progenitors. As the photosphere recedes into the core heavier elements like Oxygen, Magnesium and Iron become visible.

The nebular spectra are characterized by $H\alpha$, Oxygen and Calcium emission lines.

1.3.5. X-Ray & Radio observations

Compared to the traditional optical astronomy X-Ray & Radio are relatively new fields. The information carried in the very high and low frequency photons is invalueable to understanding various transient events.

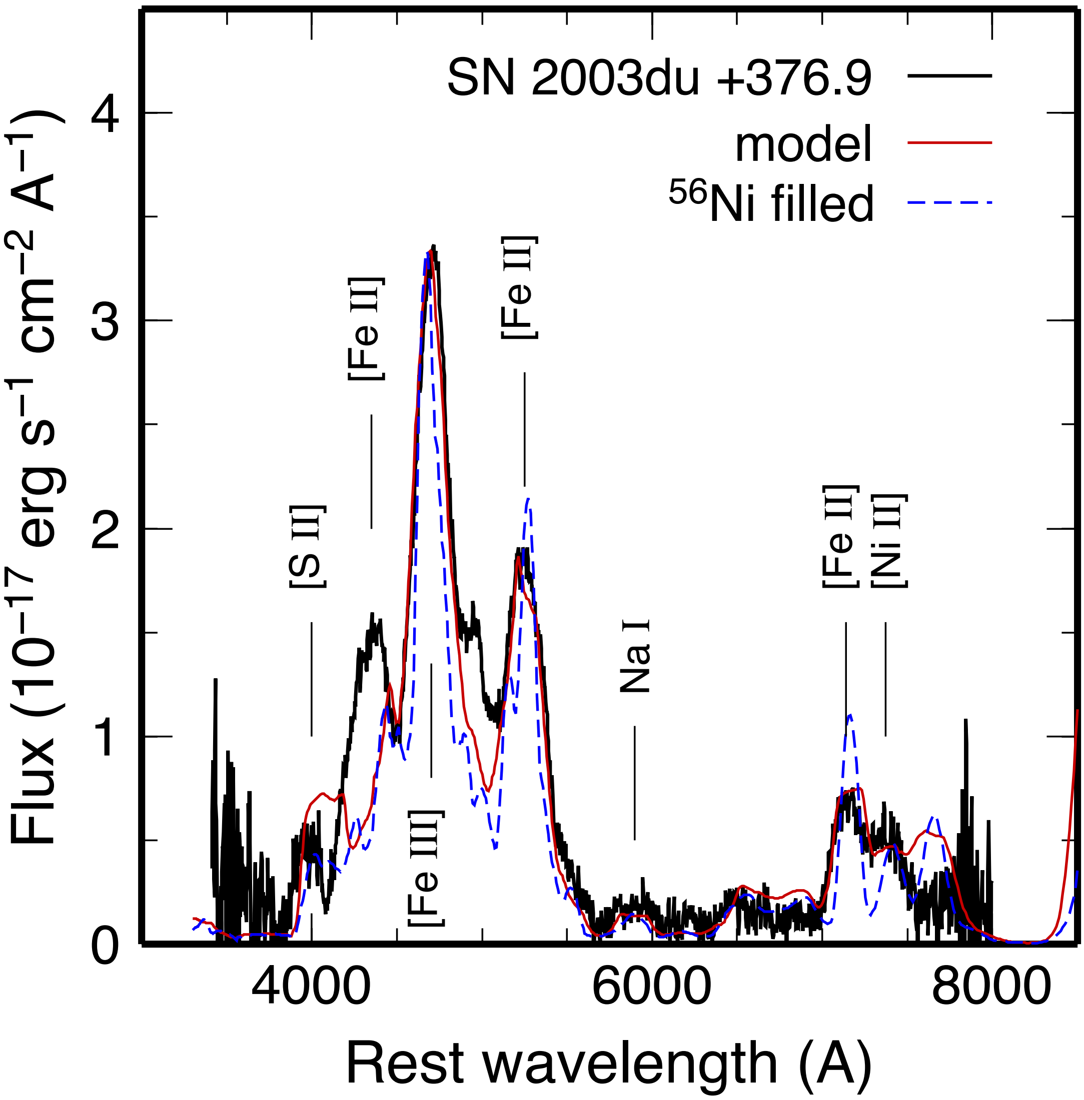

Figure 1.12 example caption

X-Ray & Radio observations in the case of SNe Ia can for example reveal the shock interaction of the ejecta with the CSM. The single degenerate scenario predicts much more CSMthan the double degenerate scenario. X-Ray (**?**) and Radio Observations (**?**) have however not revealed any emission in either Band. This could hint that the double degenerate scenario is the more common, but many caveats remain.

The long GRB-phenomenon has been suggested to be the relativistic jet launched in a SN Ib/c. In their late phase GRB's jet spreads and is thought to emit isotropically in radio. This radio glow should be visible to both on-axis and off-axis observers, but has so far only been observed on-axis . **?** have tried to find this isotropic radio emission at late times on SN Ib/cto see if they are off-axis GRBs. The study however remained inconclusive.

SNe II have long been theorized to emit X-Rays at shock breakout (**??**). To observe them is technically very challenging as the supernova needs to be detected very early on. SN2008D was serendipitously discovered as the Swift X-Raytelescope picked up an extremely luminous source. Subsequent ground based follow-up revealed a brightening optical counterpart.

Radio and X-Ray observation of both kinds of supernovae are still in its infancy and will provide great help when solving the current mysteries surrounding all types of supernovae.

1.3.6. Supernova Cosmology

Early in the last century astronomers where trying to gauge our place in the universe. The question of distances to several astronomical objects arose. A distance probe is a astronomical phenonomen Over time many distance-independent luminosity relations were discovered such as the absolute Magnitude-Period relation of Cepheids. The discovery of these standard candles lead to the creation of the field of cosmology.

Supernovae have played a vital role in discovering the current structure of the Universe

SN II Cosmology: SN IIP have been first suggested as cosmological probes by **?**. It is important for cosmological distance probes to know the intrinsic luminosity precisely. At the plateau-phase of the supernova, caused by the hydrogen-recombination, the temperature is well known (T=5000 K). In addition it is assumed that the supernova is in free expansion, thus a measurement of the velocity and an assumption of the initial radius results in a known radius. Assuming the supernova to be a blackbody during plateau-phase one can then calculate a luminosity using the radius and the temperature. SN IIPas distance candles, however, are observationally expensive and not as accurate as SN Ia as standard candles (15% error for SN II(**?**) vs 7% error for SN Ia).

SN Ia Cosmology SNe Ia have been one of the most successful distance probes. It is believed that SNe Ia are the explosion of C-O white dwarfs. The brightness of these objects is powered by the decay of ^{56}Ni. The quantity of ^{56}Ni produced in the explosion can be gauged from the evolution of the light-curve which then in turn can be used to calibrate the intrinsic brightness (see Figure **??**). In the late 1990s new detector technologies (CCDs), computing and new telescopes made it possible to measure the lightcurves of many SNe Ia accurately.

? made the discovery that more distant galaxies move at higher velocities. It was implied that the universe is in a state of constant expansion. The amazing discovery that both **?** and **?** made with SNe Ia was that the universe, in stark contrast to the earlier assumption, was expanding at an accelerating rate.

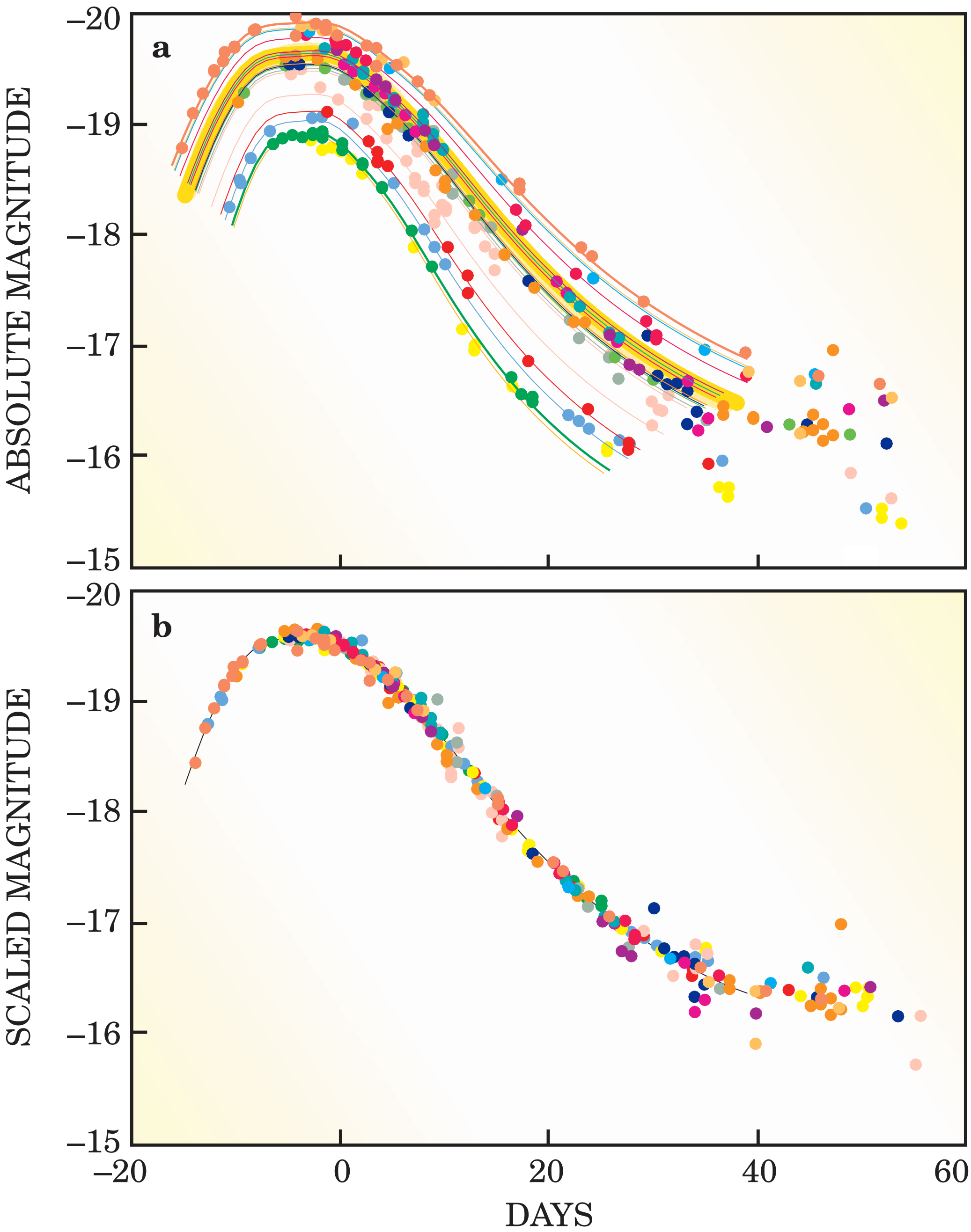

Figure 1.13 Replace with Brad data

1.4. Core-Collapse Supernova Theory

All SN II are believed to be powered by the collapse of the electron-degenerate iron core of massive stars. For the iron core to form there had to be several prior stages of evolution.

1.4.1. Evolution of Massive Stars:

To understand the state of the star shortly before supernova evolution it is imperative to follow its evolution. For the topic of SN II we will concentrate on the nuclear physics of massive star evolution in this section. In the scope of this work we will follow a single massive star as a progenitor. There has been ample suggestions that some SN II progenitors are binary, but their evolution is much more complex and is outside the scope of this work?? citation needed??. In this context massive stars are stars bigger than 8 $M_{\odot}$. This is the minimum mass for a star that is believed to explode in a SN II. Like all stars massive stars spend most of their lives on the main-sequence burning hydrogen. This happens via the carbon-nitrogen-oxygen cycle and its various side-channels (e.g $^{12}C(p,\gamma) \rightarrow^{13} N(e^{+}\nu) \rightarrow^{13} C(p,\gamma) \rightarrow^{14} N(p,\gamma)^{15}O(e^{+}\nu) \rightarrow^{15} N(p,\alpha) \rightarrow^{12} C$). For a 20 $M_{\odot}$star this phase lasts for 8.13 Myr(see **?**).

As the star evolves it begins to ignite Helium which burns via the triple-α process to Carbon ($3\alpha \rightarrow^{12} C$) and then to Oxygen ($^{12}C(\alpha,\gamma) \rightarrow^{16} O$). Table 1 in **?**) lists 1.17 Myr for this phase.

Due to neutrino losses the stellar evolution is qualitatively different after helium burning. A neutrino-mediated Kelvin-Helmholtz contraction of the carbon-oxygen core describes the advanced stages of nuclear burning in massive stars well (**?**). This is contraction is occasionally delayed when the burning of new fuel sources counter-acts the neutrino losses. The star in the end is composited of a series of shells that burn the above fuel and deposit the ashes on the shell below (see Figure **??**). There are four distinct burning stages. Their principal fuels are carbon, neon, oxygen, magnesium and silicon.

In the carbon burning stage two ^{12}C nuclei are fused to an excited state of Magnesium which then decays slowly to ^{23}Na (see **??**).

$$\begin{aligned} {}^{12}C +^{12} C \rightarrow^{24} Mg &\rightarrow {}^{23}Mg + n \\ &\rightarrow {}^{20}Ne + \alpha \\ &\rightarrow {}^{23}Na + p \end{aligned} \tag{1.1}$$

Although oxygen has a lower Coulomb barrier, the next nucleus to burn after Carbon is Neon. This layer is composed of of ^{16}O, ^{20}Ne and ^{24}Mg and burns Neon with high-energy photons from the tail of the Planck distribution (^{20}Ne$(\gamma,\alpha)^{16}$O).

In the next shell there is a composition of mainly ^{16}O, ^{24}Mg and ^{28}Si. The bulk nucleosynthetic reaction is shown in **??**.

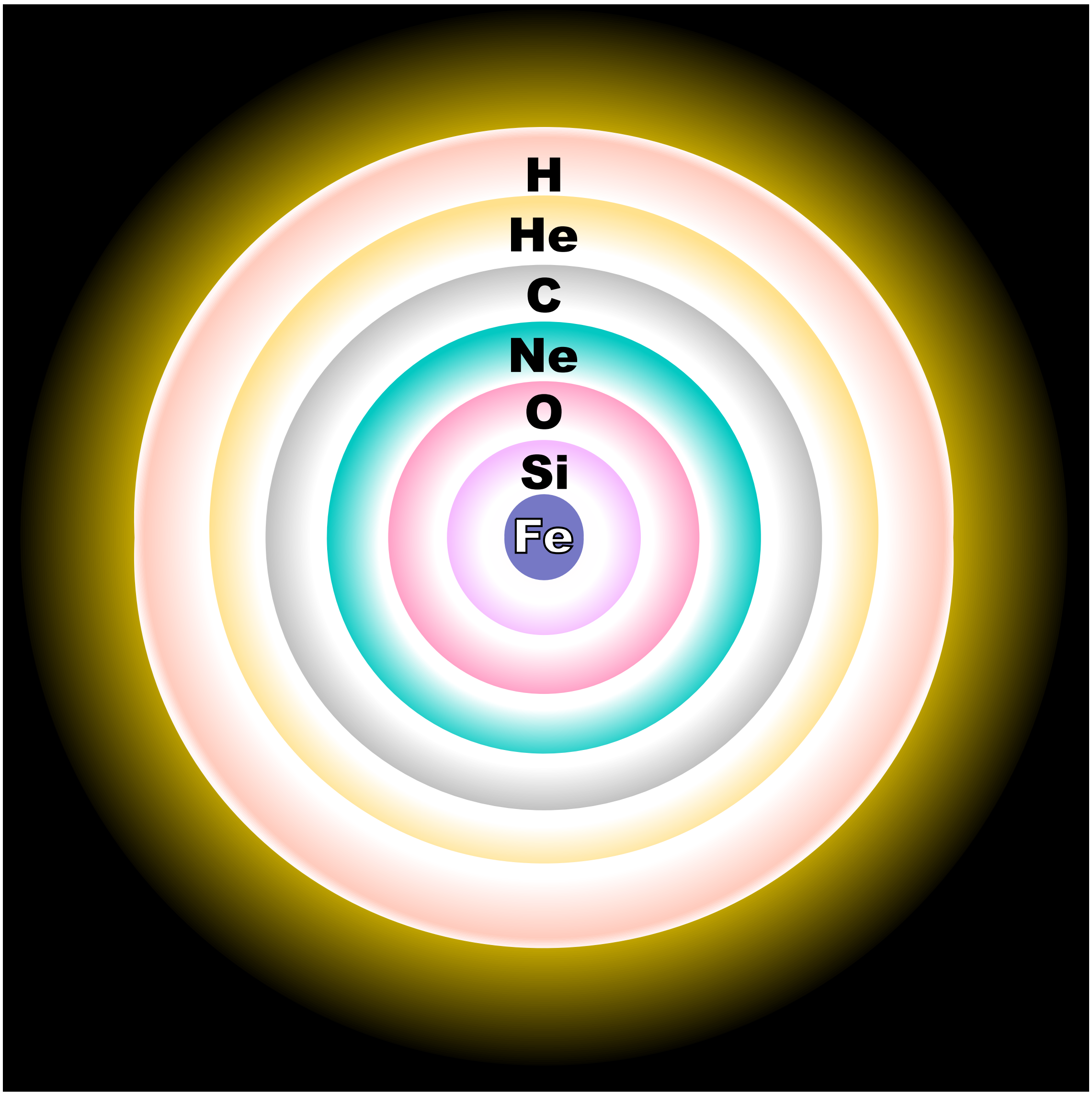

Figure 1.14 example caption

$$
\begin{aligned}
{}^{16}C +^{16} O \rightarrow^{28} Si &\rightarrow {}^{31}S + n \\
&\rightarrow {}^{31}P + p \\
&\rightarrow {}^{30}P + d \\
&\rightarrow {}^{28}Si + \alpha
\end{aligned}
\tag{1.2}
$$

The last shell is of burning ^{28}Si to ^{56}Ni is very complex. The obvious reaction $^{28}\mathrm{Si} +^{28} \mathrm{Si} \rightarrow^{56}$ Ni does not take place, but is replaced by a very complex network of isotopes to burn to ^{56}Ni. In simulations this is computationally intensive and numerically unstable (e.g . **?** who carry a 128-isotope network). Following silicon burning the composition consists of mainly iron-group nuclei. At the end of silicon burning we are reaching nuclear statistical equilibrium.

1.4.2. Core collapse

Before the collapse the core, consisting of iron peak elements. Neutrino losses during carbon and oxygen burning decreased the central entropy sufficiently so that the core becomes electron degenerate. Such a degenerate core, which is higher than the Chandrasekhar mass (adjusted for Y_e, entropy, boundary pressure and other parameters will collapse.

There are two main instabilities that facilitate the collapse. As the density rises the Fermi-Energy becomes high enough for electrons to capture onto iron-group nuclei. This capture process removes electrons that were providing degeneracy pressure and reduces the structural adiabatic index.

The second instability is the rise to temperatures where the nuclear statistical equilibrium favours free α-particles. The collapse eventually leads to nuclear densities, the hard-core potential acts as a stiff spring during the compressive phase. It stores up energy and eventually releases this energy resulting in a "core bounce". **??** believed the core bounce to provide the energy for the ensuing supernova explosion. More recent simulations however show that the bounce shock is not sufficient for a SN II explosion. The bounce shock looses energy by photo disintegrating the nuclei it encounters (loosing roughly 10^{51} erg per $0.1\,M_{\odot}$). Different neutrino flavours that the resulting neutrino winds likely play a big role.

The energy for a successful explosion is now thought to come from neutrino energy deposition. This reinvigorates the shock and leads eventually to an explosion which ejects the envelope of the massive star. A newly born neutron star is left behind.

The precise explosion mechanism is unknown. Using progenitor models with different parameters like rotation and mass lead to different outcomes. **?**provide a very comprehensive review of the theory of evolution and core collapse. In particular they lay out a more extensive description of the scenarios after core-bounce.

1.4.3. Pair instability

One explosion scenario is the pair-instability supernova. This scenario is believed to only happen in stars with a helium core of more than $40\,M_{\odot}$. After core helium burning the star starts to contract at an accelerated rate. The energy releases during this process is used to produce electron-positron pairs rather than raising the temperature. If significant densities are reached, oxygen fusion eventually halts the implosion and the collapse bounces to an explosion. For very high stellar masses it is believed that oxygen fusion does not provide enough energy to halt the contraction and the star collapses to a black hole.

1.4.4. Type II Supernovae

The observables of these stellar cataclysm are the light curve, spectra and for one case even the neutrino wind. The supernovae goes through three distinct phases which can be observed.

The shock-breakout is the first visible signal from the supernova. **?** calculated a duration for the shock breakout of SN1987A to 180 s three minutes, its luminosity of 5×10^{44}erg s^{-1}.

Thus far it has been observed only once in 2008D (**?**). They report a duration of 400 s with a luminosity of 6.1×10^{43}erg s^{-1}.

The plateau seen in many SN II (see figure **??**) is produced by the recombination of hydrogen when hydrogen-rich zones cool to less than 5500 K. The radiation comes effectively from a blackbody, whose luminosity is determined by the radius of the photosphere. Supernovae of Type IIL do not show this behaviour and are thus thought to have no or a very small hydrogen envelope.

After the recombination of hydrogen the light-curve drops off linearly and we see radio-activity providing the main energy source. ^{56}Ni decays to ^{56}Cowith a half-life of 6.1 d and then further to ^{56}Fe with a half-life of 77 d. Most of the energy of the ^{56}Nidecay is used to accelerated the expansion of the core. The tail of the light-curve after the plateau is mainly powered by the decay of ^{56}Co. Some light be also produced by shock interaction with the CSM.

1.4.5. Type Ib/c supernovae

If the star lost all of its hydrogen envelope prior to core-collapse there is no plateau visible in the light-curve. Instead the light-curve is powered by radio-active decay after shock breakout. In addition, the hydrogen lines are not visible in the spectrum. This leads to the supernova being classified as Type I. If both hydrogen and helium envelopes are lost then the supernova is classified as Type Ic. This loss of envelope is presumed to be caused by stellar winds or binary interactions (citation needed).

1.4.6. Gamma Ray Burst

1.5. Thermonuclear Supernova Theory

In this section we will discuss the theory of SNe Ia. We will, however, focus mainly on the explosion mechanism and not the theoretical implications of different progenitor scenarios. As this work is focussing considerably on SN Ia-progenitors we will dedicate a section on the different progenitor models (see **??**).

1.5.1. White Dwarfs

White dwarfs are thought to be the progenitor stars of Type Ia supernovae. These objects are among the few that do not have hydrogen, which would explain the lack of hydrogen in SN Ia-spectra. It is a general believe in the community that these objects accrete matter (for the possible scenarios see section **??**) until they get close to the Chandrasekhar-mass (**?**). It is a delicate balance between the ignition point that results in the thermonuclear run-away and the Chandrasekhar threshold which leads to a collapse of the star to a neutron star.

There are three main classes of white dwarfs: Helium, Carbon/Oxygen (henceforth CO-WD) and Oxygen/Neon/Magnesium (henceforth ONe-WD) white dwarfs. Helium white dwarfs would start burning their Helium to Carbon and Oxygen well before it gets near the Chandrasekhar mass.. In addition, these objects can also be ruled out as progenitors for SNe Iaas copious amounts of IGE produced in SNe Ia which are not consistent with the burning of a Helium white dwarf.

The ultimate fate of a ONe-WD is thought to be the collapse into a neutron star. Once the ONe-WD is heavy enough electron capture begins in the core (^{20}Ne$(e^-,\nu)^{20}$F$(e^-,\nu)^{20}$O). Heating by the resulting γ-rays starts explosive Oxygen burning. However, the electron-capture is much faster than the Oxygen burning and promotes the collapse to a neutron star (**??**).

The favoured progenitor for a SN Ia are CO-WDs. Most of these objects are born, however, with a mass around 0.6 $M_\odot$ (**?**). It is thought that they accrete mass until they are getting close to the Chandrasekhar mass and then explode as a SN Ia.

1.5.2. Pre-supernova evolution

The white dwarf gradually accretes more and more material. At some instant mild carbon burning ensues

$$\begin{aligned} {}^{12}\mathrm{C}({}^{12}\mathrm{C},p) &\rightarrow^{23}\mathrm{Na} \\ {}^{12}\mathrm{C}({}^{12}\mathrm{C},\alpha) &\rightarrow^{20}\mathrm{Ne} \\ {}^{12}\mathrm{C}({}^{12}\mathrm{C},n) &\rightarrow^{23}\mathrm{Mg} \end{aligned} \tag{1.3}$$

, but is mediated by photon and neutrino loses (**??**). As the cooling processes become less effective convection starts in the core. The energy output in the core increases. At this stage the thermal structure is largely controlled by Urca pairs. These reaction pairs consist of alternating electron captures and β^- -decays involving the same pair of parent and daughter nuclei. Two prominent examples which are important in pre-supernova evolution are ^{21}Ne/^{21}F:

$$\begin{aligned} {}^{21}\mathrm{Ne}(e^-,\nu) &\rightarrow^{21}\mathrm{F} \\ {}^{21}\mathrm{F}(\beta^-\nu) &\rightarrow^{21}\mathrm{Ne} \end{aligned} \tag{1.4}$$

These processes can lead to either cooling or heating. **?** have modelled this process in a convective core.

Ultimately, the pre-supernova evolution is hard to model theoretically as it is likely to be nonlocal, time-dependent, three dimensional and stretches over very long timescale. The exact conditions at the time of explosion are therefore unknown. All explosion models have to assume simple initial conditions.

Ignition The Urcaprocesses will dominate core evolution for the last thousand years until explosion. As the temperature rises to $T \approx 7 \times 10^8$ K (**?**) the convection time (τ_c) increases and becomes comparable to the burning time (τ_b). Consequently the convective plumes burn as they circulate. Once the temperature reaches $T \approx 10^9$ K τ_b becomes very small compared to τ_c and Carbon and Oxygen essentially burn in place. This is the moment of ignition. As the convective plumes burn while they rise it is likely that the initial flame seed does not start in the center of the core. **?** have used multiple flame seeds in their three dimensional full star models.

Thermonuclear Explosion From this point, initially there were two main options. The first option was the complete detonation (supersonic flame front) of the CO-WD (**?**). It was quickly, discovered, however that this method burns to NSEand thus produces no IME. These IMEare observed in SN Ia.

For a long time it was then suspected that the star instead of detonating would deflagrate (subsonic flame wave, mediated by thermal conduction). The fuel in front of the deflagration gets rarified by the energy from the flame. Hot light burning bubbles rise into the cold dense fuel and create Rayleigh-Taylor instabilities (see Figure **??** at t=0.72 s). Once the deflagration wave has run through the star, the resulting production of ^{56}Ni is not enough to explain the light curve of normal SN Ia. The deflagration produces roughly $0.3\,M_{\odot}$of ^{56}Ni, to power the light curve of normal SNe Ia one needs $0.6\,M_{\odot}$(**?**).

The currently favored scenario is the one of delayed detonation. The star initially burns like in the deflagration scenario, then inhomogeneities in the deflagration front produce hotspots. In these hotspots the temperature gradients are so high that detonation waves form. The ensuing detonation front can only burn the cold unburnt-fuel and does not penetrate the ashes of the deflagration. Figure **??** shows clearly how the detonation wave wraps around the cold ashes over the course of the detonation.

An open question is if and how these transitions from deflagration to detonation occur in SNe Ia. This scenario reproduces the light curves and spectra reasonably well (**?**).

sub-Chandrasekhar-mass detonations The main theme of this explosion mechanism is that a surface detonation drives a shock-wave into the core. In the core this shockwave triggers an ignition by compression. **?** have explored this scenario theoretically. As an initial model they use a CO-WDaccreting from a helium rich companion building a thin helium shell around its CO interior (described in **?**). This helium shell is ignited (maybe due to accretion) and sends out a shockwave. As the helium flame spreads on the shell around the star it sends a shockwave into the core. Once the shockwaves converge off-center they create a the right environment for the launch of a detonation wave (see Figure **??**.) The resulting detonation consumes the star. **?** have simulated the off-center detonation of a sub-Chandrasekhar-mass CO-WDand the resulting light-curve and spectra reproduce observed ones fairly well. This scenario reproduces the intrinisic luminosity variability in the class of SN Ia as each exploding white dwarf can have a different mass. An additional advantage of this model is that it is not in conflict with population synthesis predictions (**?**).

WD-WD mergers CO-WD mergers for a long time were thought to lead to a gravitational collapse (same mechanism as the ONe-WD **?**). **?** has, however, successfully simulated the explosion of two merging CO-WDs. The initial model was two equal mass $0.8\,M_{\odot}$ CO-WDs. The merging process created a hotspot from which a detonation wave eminates. The resulting light-curves and spectra are very faint but are similar to sub-luminous SN Ia(e.g. SN 1991bg).

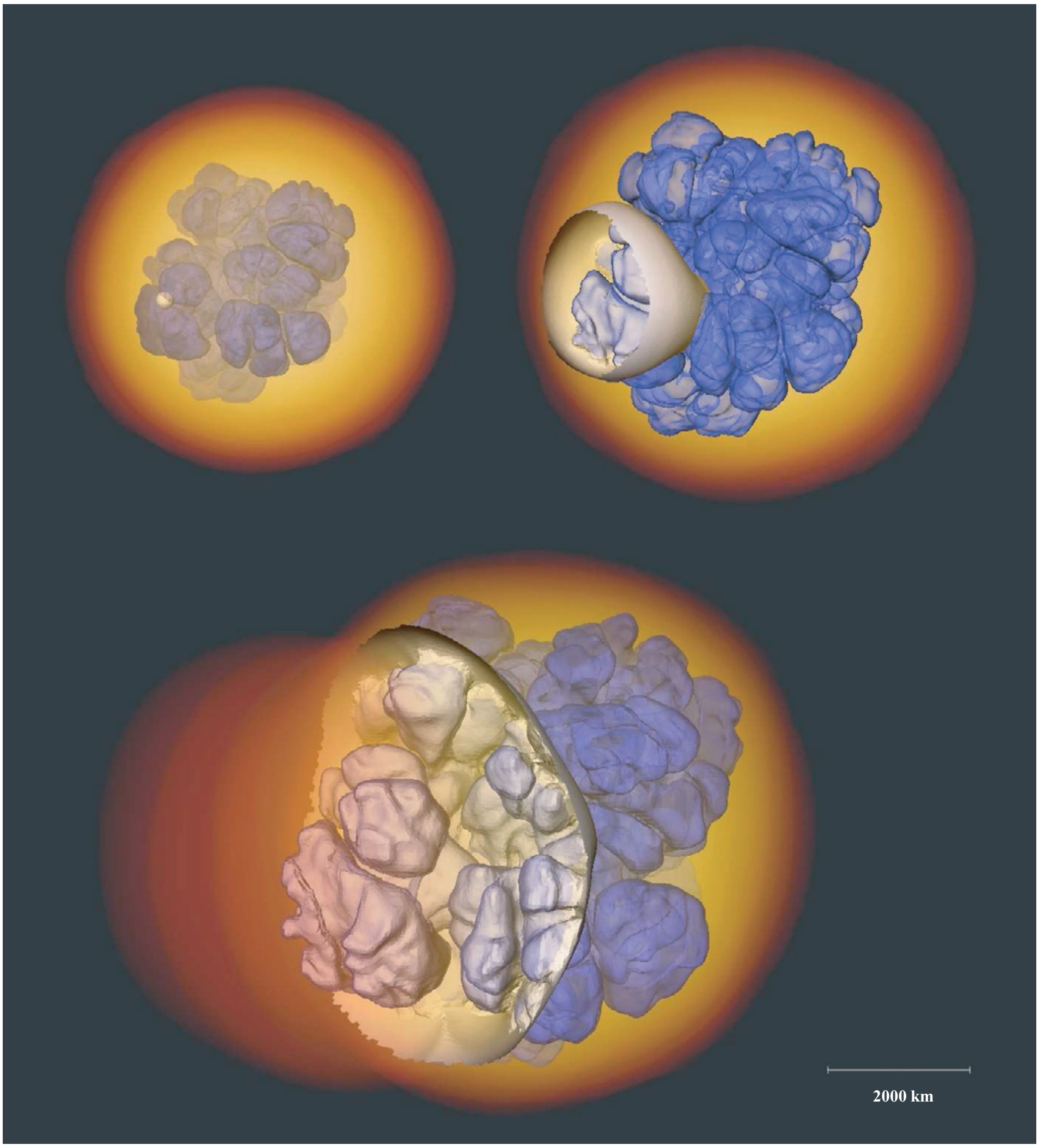

Figure 1.15 ?,(kind permission of Fritz Röpke

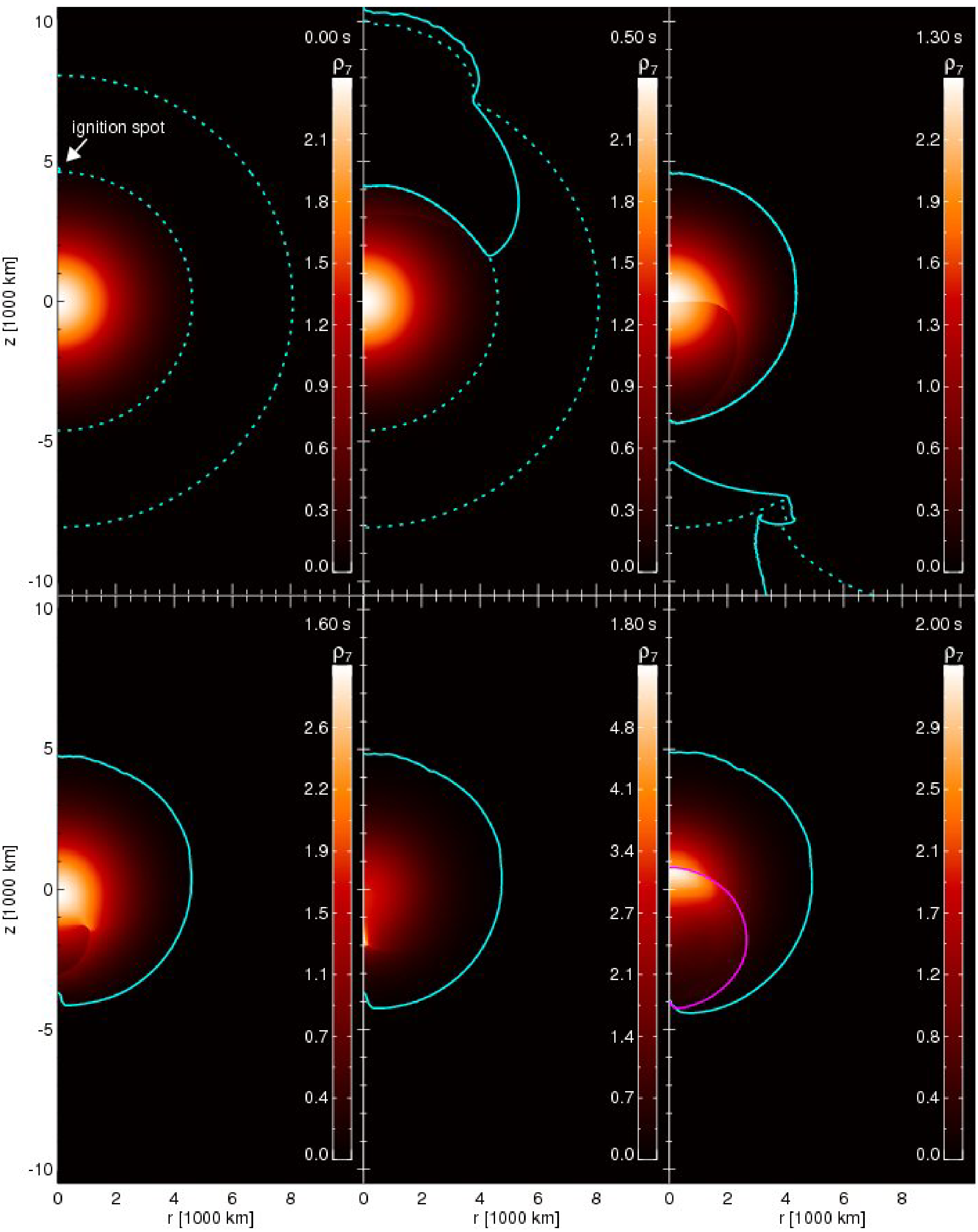

Figure 1.16 example caption

1.6. Progenitors of Type Ia Supernovae

? first introduced the modern binary evolution paradigm for SN Ia-progenitors. In their model a CO-WD accreted from a red giant. A degenerate CO-WD accreting from a non-degenerate companion is now known as the single degenerate scenario.

? were one of the first to suggest that the merging of two CO-WDs could also produce SNe Ia. This scenario is now commonly referred to as the double degenerate scenario. Embarrassingly forty years after first progenitor suggestion the progenitors of SN Ia are still not known. Without knowing the precise channel (or channels) for SN Iait is hard to make precise statements about yields, rates and explosion energies. One of this thesis main goals is finding the remaining companions in ancient SN Ia-remnants (see Chapter **??** and Chapter **??**).

1.6.1. Single Degenerate Scenario

In the single degenerate scenario assumes a binary system with one evolved white dwarf and one non-degenerate companion. In most cases this non-degenerate companion is thought to be main-sequence to red giant phase. There are scenario that involve "exotic" companions such as helium stars. The companion (or donor) star is believed to have filled its Roche-Lobe and lose mass via Roche-Lobe-Overflow (RLOF). Different scenarios see accretion from the wind of the companion rather than from RLOF (**?**).

Evolution see mennekens ....

Accretion The main problem of the SD-scenario is the accretion process. As most white dwarfs are born with masses around $1.6\,M_{\odot}$they need to accrete mass to reach the critical $1.38\,M_{\odot}$. The process needs to be efficient as well as burn most accreted hydrogen to explain its lack in the spectrum. If the mass-accretion rate is too low it causes nova explosions which eject are thought to eject more mass than they had accreted prior (**?**). There are however systems (e.g. RS Oph, U Sco) that have white dwarf masses close to $1.4\,M_{\odot}$ which have recurrent nova outbursts. It is very likely that these systems weren't born with a white dwarf that massive, but that these white dwarfs accreted all the material. This suggest that despite nova outbursts efficient accretion is possible.

A degenerate layer of helium can form at moderate accretion rates. This layer may flash and could give rise to sub-Chandrasekhar-mass explosions.

A class of binaries called Supersoft X-Ray sources (SSS) probably accrete hydrogen at a high rate. At this rate Hydrogen and Helium burn hydrostatically, if retained, make these objects very strong contenders for SN Ia progenitors. **?** however have not found enough X-ray flux from elliptical galaxies if all SN Ia-progenitors were these SSS (assuming the X-Ray flux calculated for these objects is correct).

At extremely high accretion rates the white dwarf would be engulfed in an extended red giant envelope. Debris of this envelope is not seen in SN Ia-explosions.

Another subclass of SD-progenitors are AM CVn stars. These type of cataclysmic variable accretes from a helium star. This scenario would very conveniently explain the lack of hydrogen in SN Ia-explosions. **?** have found a way that such systems can explode in a SN Ia.

Donor Stars

The SD-scenario requires a secondary companion (also known as donor) star. If this companion survives the explosion it would be a calling card for the SD-scenario.

? have simulated the impact of SN Ia-ejecta on main-sequence, sub-giant and red-giant companion. In the case of the main-sequence companion the supernova ejecta heats a small fraction (1-2%) of the envelope which is lost post-explosion. The stellar core cools and expands. It subsequently pulses while going back to hydrostatic-equilibrium. **?** have repeated the simulations for the main-sequence companion and find similar results to **?**. Post-explosion the star could be very luminous ($500 - 5000\ L_{\odot}$) due to its asymmetrical temperature distribution. It is expected to cool down between 1400 – 11000 yrs and follow the main-sequence track.

For the sub-giant companion the simulations show very similar results to the main-sequence companion. In summary, the subgiant looses only a small fraction of the envelope (10 – 15%) and will be very luminous shortly after the explosion. After thermal equilibrium is established the companion will return to a post-main-sequence track.

The case of the red-giant, however, is very different. **?** suggest that it will loose most of its loosely bound envelope. Post-explosion the remaining core rises contracts and the temperature rises to more than 3×10^4 K. The object may appear as an under luminous main-sequence O or B star.

? have suggested low-mass single white dwarfs to be the remaining cores of red-giant donor stars. This would result in a convenient explanation for the existence of these objects.

One feature of surviving companions may be an unusually large rotational velocity post-explosion (**?**, chapter **??** of this work). Due to tidal coupling during the RLOF-phase one calculate the expected rotational velocity from the escape velocity of the donor (see Figure **??**). Late-type stars usually don't display such high rotational velocities. Thus this feature is a very useful discriminant when looking for donor stars.

Most simulations suggest that the donor-star would survive the explosion one way or another. There have been several attempts to find these objects in ancient supernova remnants. **?** found a OB subdwarf star located 2.5 ′from the center of the remnant of SN1006 and suggested this as the donor star. Subsequent analysis by XXX have however revealed however strong red and blue shifted iron lines. The velocities of these lines are on order of 5000 km s^{-1}which is the same as the velocity of the freely expanding remnant of SN1006.

? have suggested a star called Tycho-G by their nomenclature as the progenitor of SN1572. (**??**, chapter **??** of this work and **??**) have followed this up and did not find Tycho-G to be very unusual to the other stars in the field.

citekerz11b have observed 80 stars in the center of SN1006 and have not found an obvious donor star..... ?????

1.6.2. Double Degenerate Scenario

? was one of the first to suggest merging white dwarfs as progenitors for SN Ia. The one big advantage of the DD-scenario is that it naturally explains the lack of hydrogen in SN Ia-spectra. The accretion problem encountered in the SD-scenario is also eleviated with DD, as long as the sum of masses of both CO-WD's is above M_{Chan}. The work in this thesis has failed to find the companion which may result from the SD-scenario. This would be a further encouragement for the DD-scenario.

The problem, however, is that most SN Ia are relatively homogeneous. It is hard to reconcile this fact with the merger of two white dwarfs with different initial masses, composition, angular momenta and different impact parameters.

? have simulated the merger of two equal-mass white dwarfs ($0.8\,M_{\odot}$). Their simulations suggest that the outcomes of these mergers would be subluminous. As the star cools after the contraction phase it may become a single Helium white dwarf.

? proposes that In summary, mergers of white dwarfs can definitley explain some of SN Ia. It is however questionable if these events are responsible for the main body of SNe Ia.

1.6.3. Population Synthesis

Population synthesis have been an important step in exploring the different progenitor scenarios. This science is still in its infancy, but results from new all-sky surveys will make this a very precise tool. **??** have explored the SN Ia-rate using different progenitor scenarios (SD, DDand AM CVn). Both suggest that the SD-scenario on its own can not explain the observed supernova rate. The DD-rate seems to be much closer to the observed frequency. Possibly a mix of all channels is required to explain the observed rate.

1.7. Thesis motivation

One of the most pivotal moments in astronomy in recent years was the discovery of the acclerating expanding universe by **?** and **?**. This discovery catapulted SNe Ia into the limelight of the astronomical community. There has been many advances in recent years in the understanding of these cataclysmic events (explosion models, rates, etc.). One critical piece of the puzzle, however, has so far eluded discovery: The progenitors of SNe Ia. This work's main aim was to find evidence for one SN Ia-progenitor scenario. The SD-scenario proposes a white dwarf accreting from a non-degenerate donor star. To the best of our knowledge this donor star is thought to survive the explosion and would be visible thereafter. We have tried to find this companion in two of three easily accessible ancient supernova remnants (SN1572 and SN1006). In chapter **??** we have obtained spectra of Tycho-G which had been suggested as the donor star of SN1572 (**?**). Although we confirmed some of the suggested parameters we could not reproduce the unusually high radial velocity which led to the claim.

We revisited SN1572 in chapter **??** with new observations of Tycho-Gand five other stars in the neighbourhood of SN1572. This resulted in Tycho-G to be not a very viable donor star (it is hard to completely rule stars out). We discovered a curious A-Star located serendiptiously right in the center of SN1572. Despite its bizarre parameters we could not reconcile this star (Tycho-B) with any feasable progenitor model. We, however, found a scenario which explains Tycho-B's features but does not involve it in SN1572.

SN1006 provides a perfect opportunity to search for progenitor stars. It is the closest known remnant of a SN Ia(2 kpc). We have obtained 80 spectra of stars close to the center of the remnant and present them in chapter **??**. Again we did not find any obvious donor stars.

We have obtained spectra of stars around SN1604 but these are not presented in this work.

Progenitor hunts provide us with information of the scenarios pre-explosion. Spectra on the other hand help to unravel the happenings during and post-explosion. mazzali et al. ??? have developed a code that can produce synthetic SN Ia-spectra from fundamental input parameters. Fitting an observed SN Ia is for the moment a manual task. This requires many days, if not weeks, of tweaking. The deluge of spectroscopically well-sampled SNe Ia from surveys is already hitting us. Manual analysis of all these spectra is impossible. The information about the explosion hidden in the spectra is, however, crucial to our understanding of these events. In chapter **??** we present our work towards automating this fitting process. We have tried a variety of algorithms to explore the vast and extremely complex search space. Working together with members of the computer science community we are exploring the use of genetic algorithms to solve this problem. This work is not finished yet, but we present preliminary methods in SN Ia-fitting in chapter ???. Once finished we can apply this method not only in fitting SN Ia, but fitting other supernovae and other areas of astronomy.

In summary, this work explores two areas of supernova physics. The hunt for progenitors has not yielded obvious candidates, but may suggest a rethinking of the "normal" SD-scenario. The automation of the supernova fitting is in its infancy stage. We have however shown that it is possible to explore the space in an automated fashion. This will hopefully yield parameters for many thousand supernovae and the next few years. The close collaboration with computer science community has shown how important cross-disciplinanry research is in this era of science.

CHAPTER 2

SN1572

2.1. Introduction

Type Ia supernovae (SNe Ia) are of broad interest. They serve as physically interesting end points of stellar evolution, are major contributors to galactic chemical evolution, and serve as one of astronomy's most powerful cosmological tools.

It is therefore unfortunate that the identity of the progenitors of SNe Ia is still uncertain. For example, without knowing the progenitors, the time scales of SNe Ia enriching the interstellar medium with iron remains highly uncertain. But it is the crippling impact on the cosmological application of these objects which is especially profound; it is impossible to predict the consequences of any cosmological evolution of these objects or even gauge the likelihood of such evolution occurring.

There is broad agreement that the stars which explode as SNe Ia are white dwarfs which have accreted material in a binary system until they are near the Chandrasekhar mass, then start to ignite carbon explosively, which leads to a thermonuclear detonation/deflagration of the star. It is the identity of the binary companion that is currently completely undetermined. Suggestions fall into two general categories (**?**):

- Single degenerate systems in which a white dwarf accretes mass from a non-degenerate companion, where the companion could be a main-sequence star, a subgiant, a red giant, or possibly even a subdwarf.
- Double degenerate systems where two CO white dwarfs merge, resulting in a single object with a mass above the Chandrasekhar limit.

The detection of circumstellar material around SN 2006X (**?**) has provided support for the single degenerate model in this case, although the lack of substantial hydrogen in several other SNe Ia (**?**) poses more of a challenge to this scenario.

These models also make different predictions for the nature of the system following the explosion. In the double degenerate case, no stellar object remains, but for a single white dwarf, the binary companion remains largely intact.

In the single degenerate case, the expected effect of the SN on the donor star has been investigated by **?**, who have calculated the impact of a SN Ia explosion on a variety of binary companions. **?** have explored many of the observational consequences of the possible scenarios, and Podsiadlowski (2003) has presented models that follow both the pre-supernova accretion phase and the post-explosion non-equilibrium evolution of the companion star that has been strongly perturbed by the impact of the supernova shell. To summarize these results, main-sequence and subgiant companions lose 10 – 20 % of their envelopes and have a resulting space velocity of 180 – 320 km s^{-1}. Red-giant companions lose most of its hydrogen envelope, leaving a helium core with a small amount of hydrogen-rich envelope material behind, and acquire a space velocity of about 10 – 100 km s^{-1}. **?** have used a binary stellar evolution code on a main-sequence star and exposed the evolved star to a SN Ia. Their simulations show that even less material is stripped due to the compact nature of a star that evolved in a binary. We will use their results where applicable.

?, henceforth RP04 have identified what might be the donor star to Tycho's SN, a SN Ia which exploded in the Milky Way in 1572. These authors presented evidence that this star, Tycho-G by their naming convention, is at a distance consistent with the Tycho supernova remnant (henceforth SNR), has a significant peculiar radial velocity and proper motion, roughly solar abundance, and a surface gravity lower than a main-sequence star. However, Tycho-G is located at a significant distance from the inferred center of the remnant, and any process that has displaced the star must preserve the remnant's nearly perfectly circular projected shape. During the final stages of refereeing of this paper we were made aware of the article by **?**, henceforth GH09, who used Keck HIRES data to better constrain Tycho-G's stellar parameters, and in addition, found an enhancement in Nickel abundance, relative to normal metal rich stars.

? have looked for Fe absorption lines from the remnant, using nearby stars as continuum sources, with the hope to better constrain the distance of these stars to the SNR. With their technique, stars in the remnant's center should show strong blue-shifted Fe absorption lines, formed by material in the expanding shell of Fe-rich material from the SN, moving towards the observer. Stars in the foreground would show no Fe absorption, and background stars both red- and blue-shifted absorption. Their study shows that Tycho-G does not contain any significant blue-shifted Fe absorption lines, suggesting that Tycho-G is in the remnant's foreground. However, these observations and their analysis, while suggestive, cannot be considered a conclusive rebuttal of Tycho-G's association with the remnant; this technique requires a significant column depth of Fe which is not guaranteed. A lack of Fe column depth may be indicated by the fact that no stars were found in the vicinity of the remnant that showed both blue- and red-shifted absorption lines.

To further examine the RP04 suggested association of Tycho-G with the SN Ia progenitor, we have obtained a high-resolution spectrum of the star using Subaru and its High Dispersion Spectrograph (**?**).

We summarize, in section 2, the observational circumstances of the Tycho remnant and any donor star, and argue in section 3 that rapid rotation is an important, previously unrealised signature in a SN Ia donor star. In section 4 we describe our Subaru observations. Section 5 covers the analysis of data and the results of this analysis. Section 6 compares the relative merit for Tycho-G being the donor star to the Tycho SN or being an unrelated background star, and in section 7 we summarize our findings and motivate future observations.

2.2. Observational Characteristics of the Tycho Remnant and Star-G

RP04 have done a thorough job summarizing the relevant details of the Tycho remnant. The remnant shows the characteristics expected of a SN Ia based on its light curve (measured by Tycho Brahe himself), chemical abundances, and current X-ray and radio emission (**?**). In figure **??** we have overlaid radio contours[1] on an optical image and have marked the position of the stars mentioned in this and RP04's work.

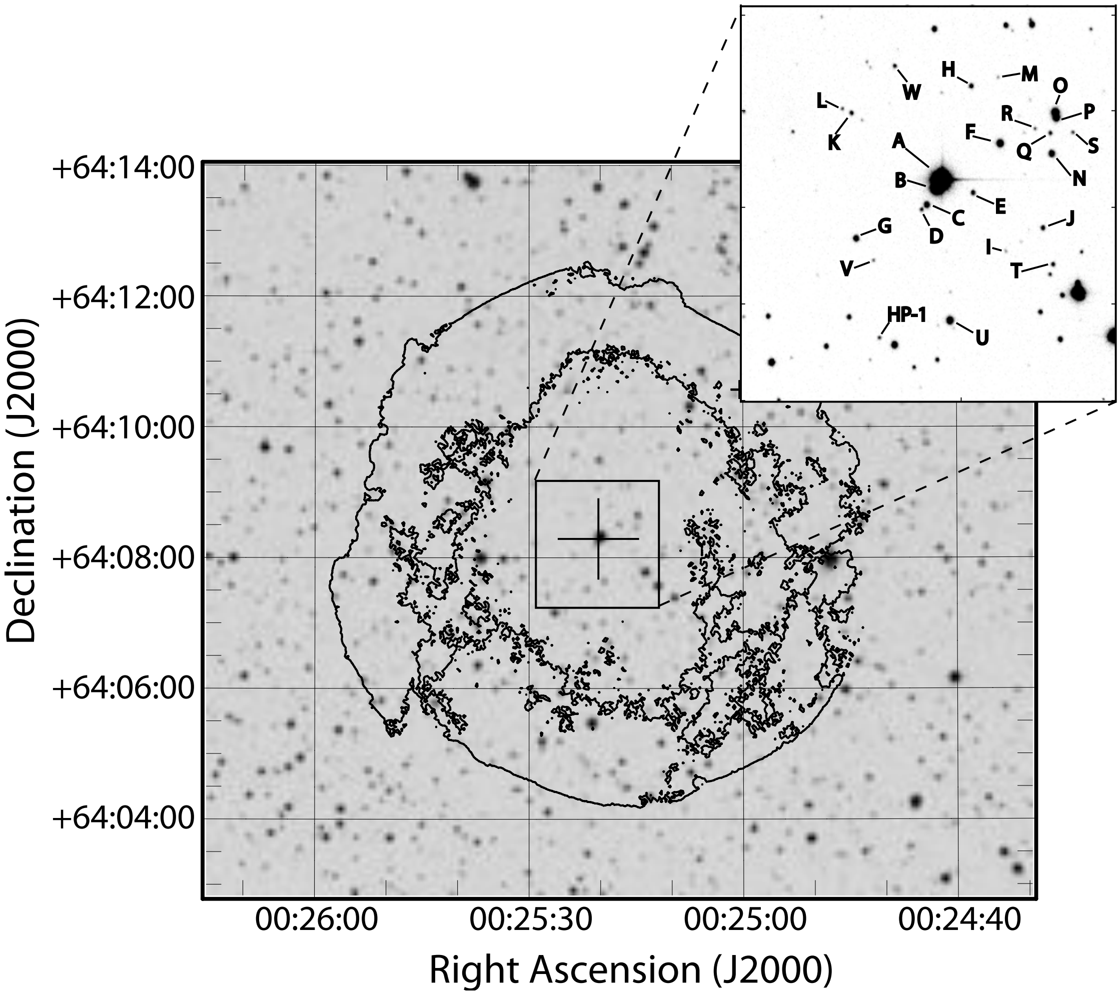

Figure 2.1 Radio Contours (VLA Project AM0347) have been overlaid (**?**) on an R-Band Image (NGS-POSS). The cutout is an INT image (see text). The stars marked in the figure are mentioned in this work and in RP04's work.

Although it is not easy to measure the remnant's distance precisely, RP04 estimated Tycho's SNR distance to be 2.8 ± 0.8 kpc, using the ratio of the SN 1006 and Tycho SNR's angular sizes and their relative ages, and the direct distance measure of SN 1006 by **?** (2003). **?** have recently shown, from a spectrum of a light echo associated with the SN1572, that this SN was a normal SN Ia. Using Tycho's observed light curve, the properties of SN Ia as standard

[1] The National Radio Astronomy Observatory is a facility of the National Science Foundation operated under cooperative agreement by Associated Universities, Inc.

candles, and an extinction value they find a distance to the SN of $3.8^{+1.5}_{-1.1}$ kpc. Updating their values for the extinction values determined in this paper (section **??**), as well as using an absolute magnitude for SN Ia of -19.5 ± 0.25 (**?**), we find a distance of $3.4^{+1.3}_{-1.0}$ kpc. In summary, we believe the remnant's distance is poorly constrained, but probably between 2 and 4.5 kpc. RP04 also report the spectroscopic and photometric properties for the bright stars near the center of the Tycho remnant and find a uniform value of approximately $E(B-V) = 0.6$ for stars more distant than 2 kpc. GH09 have revised the $E(B-V)$ value for Tycho-G to 0.76.

In addition, for a select list of stars, RP04 provide radial velocities and proper motions. For Tycho-G, RP04 report a value of $v_r = -99 \pm 6\,\mathrm{km\,s^{-1}}$ for the radial velocity in the Local Standard of Rest (henceforth LSR), a proper motion of $\mu_b = -6.1 \pm 1.3\,\mathrm{mas\,yr^{-1}}$, $\mu_l = -2.6 \pm 1.3\,\mathrm{mas\,yr^{-1}}$, $\log g = 3.5 \pm 0.5$, and $T = 5750\,\mathrm{K}$. Using HIRES data GH09 have improved the measurements of Tycho-G's stellar parameters, finding $v_r \approx -80\,\mathrm{km\,s^{-1}}$, $\log g = 3.85 \pm 0.3$, $T = 5900 \pm 100\,\mathrm{K}$, and $[\mathrm{Fe/H}] = -0.05 \pm 0.09$ dex. We note that **?** have classified Tycho-G as an F8V star ($T \approx 6250\,\mathrm{K}$, $\log g \approx 4.3$, **?**), in significant disagreement with the RP04 temperature and gravity. We believe the GH09 values are based on by far the best data, and for the purpose of this paper, we will adopt their values.

Based on the observations, RP04 asserted that Tycho-G was located at approximately 3 ± 0.5 kpc – consistent with the remnant's distance. They note that this star has solar metallicity, and therefore its kinematic signature was not attributable to being a member of the Galactic halo. They further argued that Tycho-G's radial velocity and proper motion were both inconsistent with the distance, a simple Galactic rotation model, and the star being part of the disk population of the Milky Way. The derived physical characteristics of the system were nearly identical to what was proposed by Podsiadlowski (2003) for a typical SN Ia donor star emerging from a single degenerate system (e.g., U Sco; also see **?????**). The revision in the stellar parameters by GH09 leads to different distance with a larger uncertainty, but by and large, has not altered the conclusions above. Taken in total, the data provide a rather convincing case for the association of Tycho-G with the Tycho SN.

2.3. Rapid Rotation: A Key Signature in SN Ia Donor Stars

In the single degenerate SN Ia progenitor channel, mass is transferred at a high rate from a secondary star onto a white dwarf (**??**). These high mass-transfer rates require that the secondary star overflows its Roche lobe. Due to the strong tidal coupling of a Roche-lobe filling donor, the secondary is expected to be tidally locked to the orbit (i.e., have the same rotation period as the orbital period). At the time of the SN explosion, the donor star is released from its orbit, but will continue with the same space velocity as its former orbital velocity and continue to rotate at its tidally induced rate.

There is a simple relationship between the secondary's rotation velocity ($v_{\mathrm{orb},2}$) and its orbital velocity:

$$v_{\mathrm{rot}} = \frac{M_1 + M_2}{M_1} f(q)\, v_{\mathrm{orb},2},$$

where $f(q)$ is the ratio of the secondary's Roche-lobe radius to the orbital separation (e.g.,

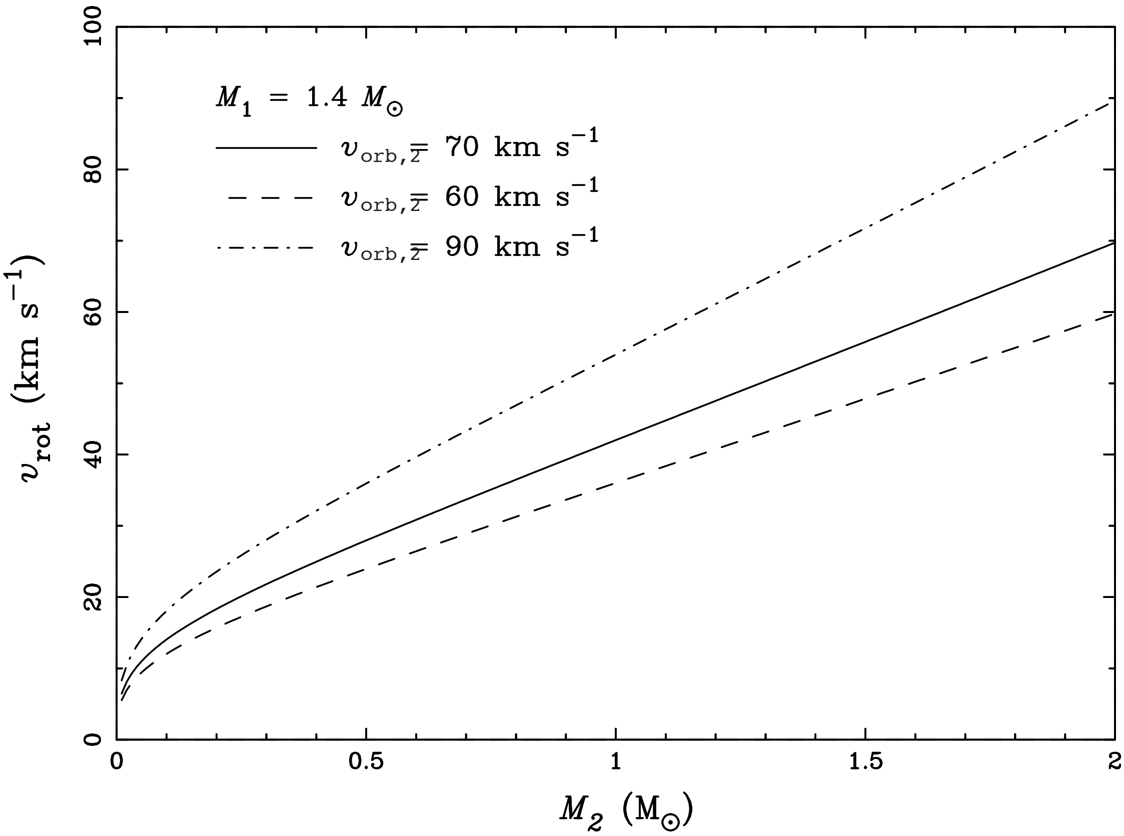

Figure 2.2 The expected rotation rate for a donor star as a function of its mass at the time of the explosion. The three curves show the results for 3 final space velocities of the donor star (similar to those suggested by RP04). It is assumed that the white dwarf has a mass of $1.4\,M_\odot$.

given by **?**) and $q = M_1/M_2$ is the mass ratio of the components at the time of the explosion. Figure **??** shows the rotational velocity as a function of secondary mass for several values of $v_{\rm orb,2}$ (consistent with RP04s measurement, and at the low end of values expected for a subgiant star), where we assumed that the exploding white dwarf had a mass of $1.4\,M_\odot$.

This estimate is strictly speaking an upper limit, as it does not take into account the angular-momentum loss associated with the stripping of envelope material by the supernova and any bloating due to the supernova heating. The latter would reduce the rotational velocity to first order by a factor equal to the bloating factor (i.e. the ratio of the new to the old radius), but the star would likely find itself in a state where its radius and temperature was atypical of a normal star.

According to the results of **?**, mass stripping is not likely to be significant if the companion is a main-sequence star or a subgiant. Furthermore, following binary evolution of a main-sequence star, **?** have shown that even less material is stripped. However, if the companion is a giant, it would be stripped of most of its envelope. Such a star would not show any signs of rapid rotation since the initial giant would have been relatively slowly rotating; e.g., if one assumes solid-body rotation in the envelope, the rotation velocity at $\sim 1\,R_\odot$ will only be $\sim 0.5\,{\rm km\,s^{-1}}$ for a pre-SN orbital period of 100 d. Moreover, the material at the surface may have expanded from its original radius inside the giant, further reducing the rotational velocity. However, if the stripping is less than estimated by **?**, then it is possible for the signature of rotation to persist for a giant, albeit at a much lower velocity.

? also showed that due to the interaction of the SN blast wave with the companion, the secondary may receive a moderate kick of up to a few $10\,\mathrm{km\,s^{-1}}$, but this kick is generally much lower than $v_{\mathrm{orb,2}}$ and therefore does not significantly affect the resulting space velocity.

Finally, we note that the observed rotation velocities are reduced by a factor $\sin i$, where i is the inclination angle. However, because the donor star's rotational axis can be assumed to be parallel to its orbital axis, a minimum observed rotation speed can be computed from the observed peculiar radial velocity (observed radial velocity minus the expected radial velocity of an object at that distance and direction). It is only if the orbital motion (and hence final systemic velocity) is solely in the plane of the sky, that $\sin i$, and therefore, the observed rotation, approaches zero.

2.4. Subaru Observations

To investigate the rotational properties of Tycho-G, we were granted time with the Subaru telescope. Our observations of Tycho-G were taken in service mode on the nights of 2005 10 17 and 2005 10 18. 9 spectra were taken with the High Dispersion Spectrograph (HDS, **?**) with a resolution of $R \simeq 40000$ (measured using the instrumental broadening of the Thorium-Argon arc lines), an exposure time of 2000 seconds each (totalling to 5 hours) and a signal to noise ratio of about 10 per pixel (measured at 8300 Å with 0.1 Å pixel^{-1}) . The HDS features two arms, with each arm feeding a 2-chip CCD mosaic. The blue arm covers 6170 Å to 7402 Å and the red arm 7594 Å to 8818 Å. An OG530 filter was used to block contamination from light blueward of our observing window, and data were binned by 4 in both the spatial and spectral directions, resulting in a pixel size of 0.1 Å (at 8000 Å) by $0.55''$.

Data were pre-processed using tools provided by the HDS team and then bias-subtracted. We created a mask from bias and flatfielded frames, where we isolated the echelle orders and flagged bad pixel regions. The data were flatfielded using internal quartz flats, and the 2-D images cleaned of cosmic rays (and checked carefully by eye to ensure there were no unintended consequences) using an algorithm supplied by M. Ashley (private communication). The spectrum of each echelle order was extracted using IRAF[2] echelle routines, with wavelength calibrations based around low-order fits of a Thorium-Argon arc. Wavelength calibration of each extracted spectrum was checked against atmospheric O_2, and our solutions were found to be accurate in all cases to within $1\ \mathrm{km\ s^{-1}}$ (**?**). Unfortunately, we lacked a smooth spectrum standard star for setting the continuum, and we resorted to calculating a median of the spectra (6 Å window) and dividing the spectra through this smoothed median. This unusual method was chosen over the common approach of fitting the spectrum with a polynomial, due to the special characteristics of this observation (low signal to noise ratio, and a complex instrumental response). While this does not affect the narrow lines our program was targetting, it does affect broad lines such as the Hα and the

[2]IRAF is distributed by the National Optical Astronomy Observatory, which is operated by the Association of Universities for Research in Astronomy (AURA) under cooperative agreement with the National Science Foundation.

CaII IR triplet. The final step was to combine all spectra and remove any remaining cosmic rays (in the 1D spectra) by hand.

2.5. Analysis and Results

2.5.1. Rotational measurement

To attain the rotational velocity of the candidate star, we measured several unblended and strong (but not saturated) Fe I lines in the spectrum (**?**). Since our spectrum only had a combined signal to noise ratio of approximately 10, we added the spectra of the lines after normalizing them to the same equivalent width. As a reference we created three synthetic spectra (one broadened only with the instrumental profile, the others with the instrumental profile and $v_{\rm rot} \sin i$ of 10 and 15 km s^{-1} respectively) with the 2007 version of MOOG (**?**), using GH09's temperature, gravity and metallicity. We use a standard value of $\beta = 3/2$ for the limb darkening although the choice of this value is not critical, which we confirmed by checking our results using significantly different values of β. Figure **??** shows the comparison between the synthetic spectra of different rotational velocity and the spectrum of Tycho-G. We have scaled the synthetic spectrum using the equivalent width. This comparison indicates that the stellar broadening (rotational, macro turbulence, etc.) is less than broadening due to the instrumental profile of 7.5 km s^{-1}, and therefore we adopt 7.5 km s^{-1} as our upper limit to the rotation of the star. If one were to adopt RP04's measurements of the peculiar spatial motion, it could be concluded that $\sin i$ is much closer to 1 than 0 (see the end of section **??** for further explanation) and thus that the rotational speed is $v_{\rm rot} \lesssim 7.5$ km s^{-1}.

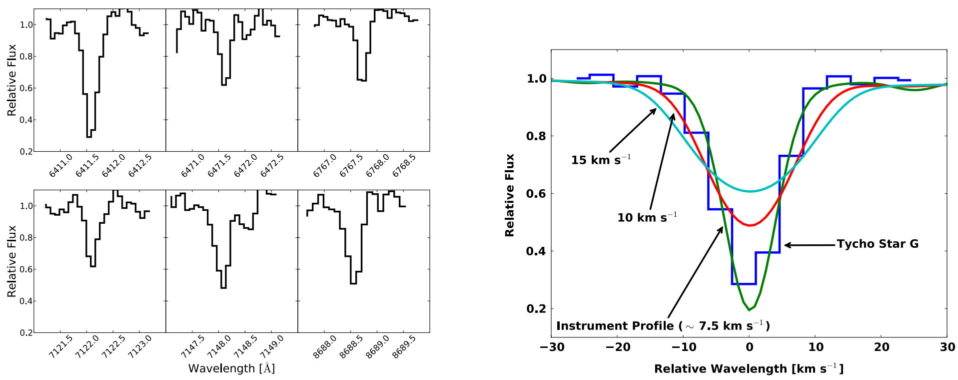

Figure 2.3 Six observed Fe I line profiles of Tycho-G are shown on the left panel. The right panel shows the combination of these line profiles after normalization to the same equivalent width and compares them to the spectrum of the Sun, which is convolved with 3 different values for the rotational broadening kernel. Tycho-G does not show significant rotation, indicating $v_{\rm rot} \sin i \lesssim 7.5$ km s^{-1}.

2.5.2. Radial velocity

To determine the radial velocity, we used 63 lines to measure the shift in wavelength. We find a radial velocity in the topocentric (Mauna Kea) frame of reference of $v_{\rm top}$ =

$-92.7 \pm 0.2\,\mathrm{km\,s^{-1}}$(the error being the standard deviation of 63 measurements) . The conversion from the topocentric to the Galactic LSR for our observations was calculated to be 13.6 km s^{-1} (IRAF task rvcorrect) using the IAU standard of motion. Including the uncertainty in the LSR definition, we find a radial velocity in the LSR for Tycho-G of $v_{\mathrm{LSR}} = -79 \pm 2\,\mathrm{km\,s^{-1}}$. This is in significant disagreement with that reported by RP04, but agrees with the revised value published by GH09.

2.5.3. Astrometry

RP04 have measured a significant proper motion for Tycho-G of $\mu_b = -6.1 \pm 1.3\,\mathrm{mas\,yr^{-1}}$, $\mu_l = -2.6 \pm 1.3\,\mathrm{mas\,yr^{-1}}$. Because Tycho-G is metal rich, and at a distance of $D > 2$kpc, this measurement provides one of the strongest arguments for Tycho-G being the donor star to Tycho SN. It is almost impossible to account for this proper motion, equivalent to a $v_b = 58\left(\frac{D}{2\,\mathrm{kpc}}\right)$km s^{-1} or 3 times the disk's velocity dispersion of $\sigma_z = 19$km s^{-1}, except through some sort of strong binary star interaction.

However, the HST data present an especially difficult set of issues in obtaining astrometry free of systematic errors. For Tycho-G these issues include the PSF on the first epoch WFPC2 image being grossly undersampled, both the ACS and WFPC2 focal planes being highly distorted, poor and different charge transfer efficiency across the two HST images, and that Tycho-G was, unfortunately, located at the edge of one of the WFPC2 chips, making it especially difficult to understand the errors associated with it. Smaller issues include the small field of overlap between the two images, making the measurement subject to issues of the correlated motions of stars, especially in the μ_l direction.

To cross-check RP04's proper motion of Star-G , we have scanned a photographic plate taken in September 1970 on the Palomar 5 meter, and compared this to an Isaac Newton 2.5 m Telescope (INT) CCD archive image (INT200408090414934) of the remnant taken in August 2004. The Palomar plate has an image FWHM of 1.7″, and the INT image 0.88″. While our images have a much larger PSF than the HST images, the images have significantly less distortion, are matched over a larger field of view with more stars, have fully sampled PSFs, and were taken across nearly an 8 times longer time baseline. The photographic nature of the first epoch does add complications not present in the HST data. The non-linear response of photographic plates causes their astrometry to have systematic effects as a function of brightness (**?**), especially affecting objects near the plate limit, where single grains are largely responsible for the detection of an object.

The position of stars on the INT image were matched to the 2MASS point source catalog (**?**) to get a coordinate transformation (pixel coordinates to celestial coordinates) using a 3rd-order polynomial fit with an RMS precision of 40 mas with 180 stars. This fit is limited by precision of the 2MASS catalog and shows no systematic residuals as a function of magnitude, or position. Using this world coordinate system (WCS) transformation, we then derived the positions of all stars on the INT image. The coordinates of 60 uncrowded stars on the Palomar plate were matched to the INT-based catalog, and a 3rd-order polynomial was used to transform the Palomar positions to the INT-based positions. The fit has an RMS of 65 mas in the direction of galactic longitude, and 45mas in the direction of galactic latitude. We believe the larger scatter in the direction of Galactic longitude is due to the shape of the PSF being slightly non-symmetric in the direction of tracking on the Palomar plate. This tracking (in RA, which is close to the direction of galactic longitude), causes the position of stars to depend slightly on their brightness. This explanation is supported by a small systematic trend in our astrometric data in μ_l, not seen in μ_b, as a function of m_R. An alternative explanation is that the trend in μ_l is caused by the average motion of stars changing due to galactic rotation as a function of distance, which is proxied by m_R. We have used the Besançon Galactic model (**?**) to estimate the size of any such effect, and find the observed effect is an order of magnitude larger than what is expected. The systemic difference between assuming either source of the observed effect is less than 1 mas yr^{-1} in μ_l, and has no effect in our μ_b measurement. In our final proper motions, presented in table **??**, we remove the systematic trend as a function of m_R with a linear function.

Table 2.1 Proper motions of stars within 45″ of the Tycho SNR center.

α [hh:mm:ss.ss]	δ [dd:mm:ss.ss]	μ_l [mas yr^{-1}]	μ_b [mas yr^{-1}]	m_R [mag]	θ [arcsec]	Name
00:25:20.40	+64:08:12.32	-0.90	-0.56	17.05	08.9	c
00:25:18.29	+64:08:16.12	-4.25	-0.81	18.80	10.0	e
00:25:17.10	+64:08:30.99	-1.82	1.78	16.87	20.3	f
00:25:23.58	+64:08:02.02	-1.58	-2.71	17.83	31.1	g
00:25:15.52	+64:08:35.44	1.94	0.83	20.28	31.4	r
00:25:15.08	+64:08:05.95	-0.67	1.49	18.86	33.3	j
00:25:23.89	+64:08:39.33	-0.31	1.08	19.20	33.5	k
00:25:14.74	+64:08:28.16	2.60	1.46	17.45	33.5	n
00:25:14.81	+64:08:34.22	4.05	-2.05	19.35	35.0	q
00:25:13.79	+64:08:34.50	2.32	1.01	19.90	41.3	s
00:25:14.59	+64:07:55.10	-3.94	2.35	19.23	41.7	t
00:25:19.25	+64:07:38.00	1.75	-3.43	16.86	42.1	u
00:25:22.45	+64:07:32.49	81.29	-2.68	19.81	48.7	HP-1

To measure the proper motion of each star, we exclude each star from the astrometric transformation fit so as not to bias its proper motion measurement. Comparing the stellar positions in the 34 year interval we find that these 60 stars show an RMS dispersion $\sigma_{\mu_l} = 2.1$mas yr^{-1}, $\sigma_{\mu_b} = 1.6$ mas yr^{-1}. For Tycho-G we measure $\mu_l = -1.6 \pm 2.1$ mas yr^{-1}, $\mu_b = -2.7 \pm 1.6$ mas yr^{-1}; this implies that no significant proper motion is detected. We do note that this measurement has a similar precision to that of RP04, is consistent with no observed motion, and is in moderate disagreement with the RP04 measurement.

In table **??** we present our astrometric measurements of all stars listed by RP04 for which we were able to measure proper motions. We also give the apparent magnitudes in R (partly measured by this work and partly by RP04) and the distance from center θ. Due to crowding caused by the relatively poor resolution of the first epoch photographic plate, several stars are not included that could be measured using HST. We include an additional star, not cataloged by RP04, which exhibits high proper motion. This high proper motion star, which was off the WFPC2 images of RP04, we designate HP-1, and has a proper motion of $\mu_l = 81.3$, $\mu_b = -2.7$ mas yr^{-1}. Due to the distance from the remnant's center, (we estimate HP-1 would have been located 51″ from the remnant's center in 1572), we doubt this star is connected to the Tycho SN, but we include it for the sake of completeness.

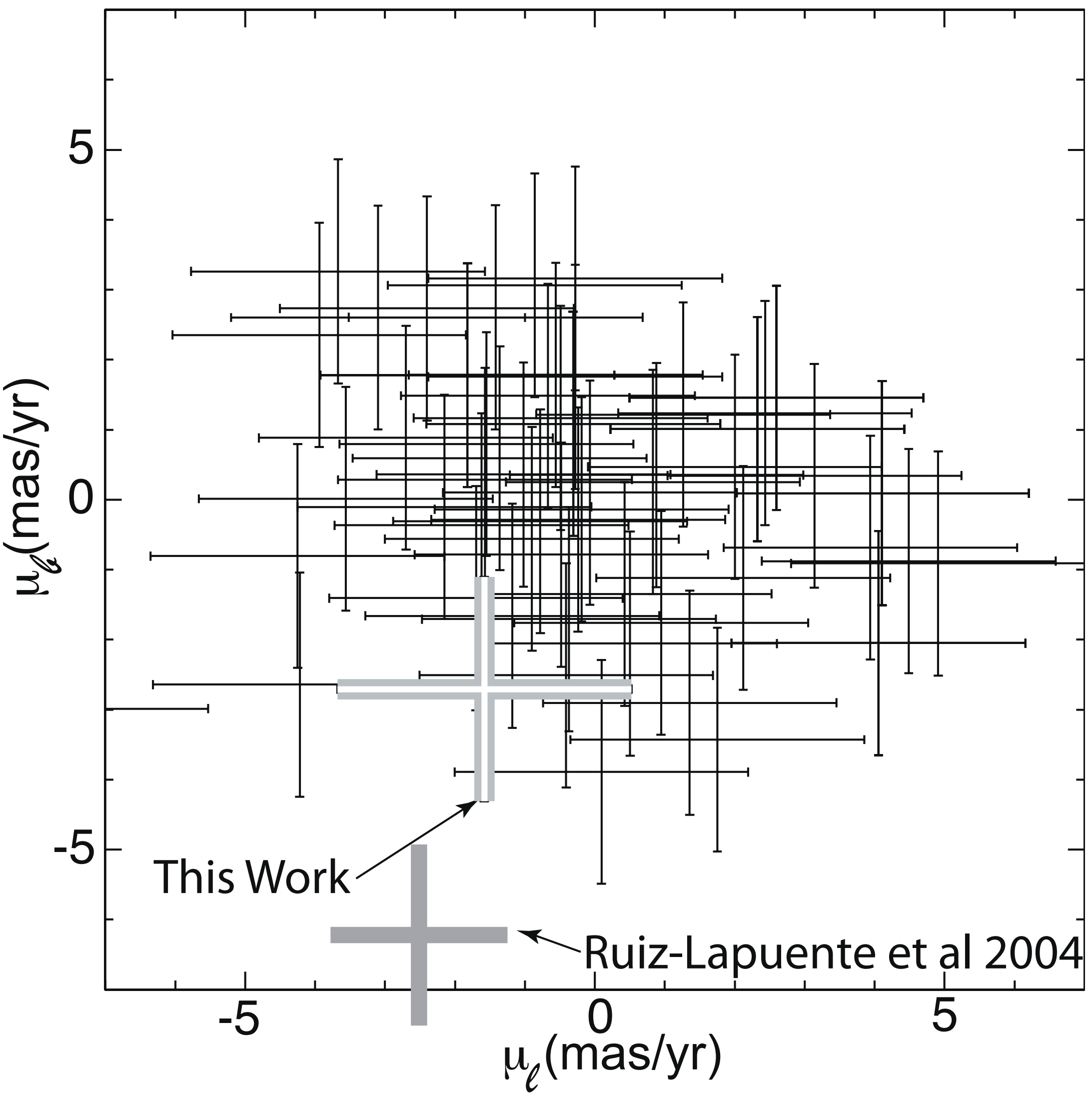

Figure 2.4 The astrometric motions of 60 stars measured in the Tycho SNR center. The measurements have a RMS dispersion of 1.6 mas yr^{-1}. Shown in grey is the proper motion of Tycho-G measured here and by RP04, showing a moderate discrepancy in the two measurements. Our measurement is consistent with no proper motion.

2.6. Discussion

2.6.1. A Background interloper?

A previously unrecognized property for many progenitor scenarios is the rapid post-explosion rotation of the donor (as described in section **??**). The expected rotation as calculated in Figure **??** is large compared to that expected of stars with a spectral type later than F and should be easily observable. We have shown Tycho-G's rotation to be less ($v_{\rm rot} \sin i \lesssim 7.5\,{\rm km\ s^{-1}}$) than what is expected of an associated star if the companion was a main-sequence star or subgiant. A red giant scenario where the envelope's bloating has significantly decreased rotation could be consistent with our observation of Tycho-G, and this will be discussed in section **??**.

The primary basis for which RP04 selected Tycho-G as a candidate for the donor star to the Tycho SN was the combination of its large peculiar radial velocity and its observed proper motion. In Figure **??** we use the Besançon Galactic model (**?**) to construct an expected set of radial velocities for metal-rich stars in the direction of SN1572.

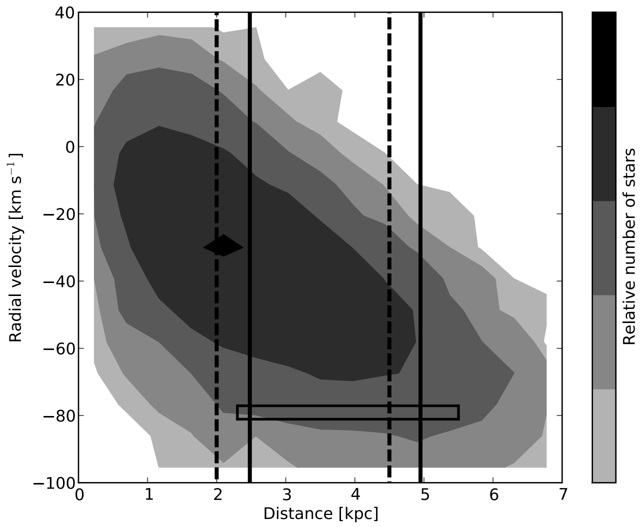

Figure 2.5 Besançon model for a metal rich ([Fe/H] > -0.2) Galactic population between 0 and 7 kpc in the direction of Tycho SNR (l = 120.1, b=1.4) with a solid angle of 1 square degree. The remnant's distance is represented by the black dashed lines (as calculated in section **??**). The contours show the radial velocity distribution. Our measured radial velocity corrected to LSR and our distance are shown, with their respective error ranges, as the black rectangle. The distance range calculated by GH09 are indicated by the two solid lines. The observed LSR v_r for Tycho-G is mildly unusual for stars at the remnant's distance, and is consistent with the bulk of stars behind the remnant.

Measuring the distance to Tycho-G is a key discriminant in associating the star to the SN explosion. To improve the uncertainty of the distance to the star, due both to temperature and extinction uncertainty, we base our distance on the observed m_K (**?**) and $(V-K)$ color (RP04). We interpolate ATLAS9 models without overshoot (**?**) to find a theoretical $V-K$ and absolute magnitude for the GH09's values of temperature and gravity. Using a standard extinction law (**?**) ($A_V = 3.12E(B-V)$ and $A_K/A_V = 0.109$) to match the theoretical and observed colors, we find $A_V = 2.58 \pm 0.08$mag, $A_K = 0.28 \pm 0.01$ mag, and $E(B-V) = 0.84 \pm 0.05$. To better show the uncertainties, we present our distance moduli scaled to the observed and derived values of extinction, temperature and gravity. The temperature coefficients were determined by integrating blackbodies of the appropriate temperature with a filter bandpass and fitting a powerlaw to the resulting flux.

$$
\begin{aligned}
(m_V - M_V) = 12.93 - 3.12(E(B-V) - 0.84) - 2.5(\log g - 3.85) + \quad (2.1)\\
+2.5\log\left(\frac{M}{1\,M_\odot}\right) + 2.5\log\left(\frac{T_{\rm eff}}{5900}\right)^{4.688}\\
(m_K - M_K) = 12.93 - 0.275(E(B-V) - 0.84) - 2.5(\log g - 3.85) + \quad (2.2)\\
+2.5\log\left(\frac{M}{1\,M_\odot}\right) + 2.5\log\left(\frac{T_{\rm eff}}{5900}\right)^{1.937}
\end{aligned}
$$

Assuming a companion mass of $1\,M_\odot$ we find a $(m-M) = 12.93 \pm 0.75$ mag. This uncertainty is dominated by the precision of $\log g$, and equates to a distance of $D = 3.9 \pm 1.6$kpc. Tycho-G, within the errors, is at a distance consistent with the remnant. As seen in Figure **??**, the observed radial velocity of Tycho-G is consistent with a significant fraction of stars in its allowed distance range. We also note that if Tycho-G is indeed associated with the SN, that it is likely that Tycho-G could have a mass considerably less than $1\,M_\odot$, due to mass transfer and subsequent interaction with the SN, although in this case, the distance to the star would still be consistent with SNR distance.

? looked for absorption due to Fe I in the remnant's expanding ejecta for 17 stars within the Tycho remnant. No such absorption was seen in the spectrum of Tycho-G, potentially placing it in front of the remnant. However, the amount of Fe I currently within the remnant is uncertain with predicted column densities spanning several orders of magnitude ($0.02 - 8.9 \times 10^{15}$ cm^{-2}; **??**). Therefore, we do not believe the lack of significant Fe I 3720 absorption in Tycho-G to be significant.

In summary, we find that Tycho-G's radial velocity, distance, and stellar parameters are all consistent with an unrelated star, but also with it being the donor star. There is disagreement in Tycho-G's measured proper motion. The measurements of RP04 are inconsistent with normal disk stars at the known distance and strongly point to Tycho-G being associated with the SN, whereas the measurements presented here are consistent with a normal disk star, unrelated to the SN. In addition, we have shown the rotation of Tycho-G is low (confirmed by GH09; $v_{\rm rot} \leq 6.6$ km s^{-1}), arguing against association with the SN, as does its off center placement in the remnant. Finally, GH09 have presented evidence that Tycho-G is strongly enhanced in Nickel, an observation that, if confirmed, would strongly point to an association of the star with the SN. If either the high proper motion, or significant Nickel enhancement can be confirmed, then it is likely that Tycho-G is the SN donor star. Otherwise, we believe it is much more likely that Tycho-G is simply an interloper.

2.6.2. Tycho-G as the Donor Star to the Tycho SN

While the case for Tycho-G's association with the SN is not conclusive, it is intriguing, and we believe it is worthwhile to look for a consistent solution assuming the association is true. While not apriori probable, a self-consistent model can be constructed in which Tycho-G was the companion, as we shall discuss now.

To make such a model work, Tycho-G has to be a stripped giant that presently mimics a G2IV star. At the time of the explosion, the star would have been a moderately evolved giant (in a binary with an orbital period ~ 100 d). The SN ejecta will strip such a giant of almost all of its envelope (?) due to its low binding energy; only the most tightly bound envelope material outside the core will remain bound. Due to the heating by the SN, even this small amount of material (perhaps a few $\times 0.01\,M_\odot$) will expand to giant dimensions, and the immediate-post-SN companion will have the appearance of a luminous red giant. However, because of the low envelope mass, the thermal timescale of the envelope is sufficiently short that it can loose most of its excess thermal energy in 400 years and now have the appearance of a G2IV star (?).

A lower mass for Tycho-G ($0.3 - 0.5\,M_\odot$) also reduces the distance estimate, and makes the observed radial velocity more unusual for stars at this distance. The expected spatial velocity depends on the pre-SN orbital period and should be in the range of $30 - 70\,\mathrm{km\,s^{-1}}$ for a period range of $20 - 200\,\mathrm{d}$ (?). These velocities are consistent with the inferred spatial velocity of the object relative to the LSR if Tycho-G is at the distance of the remnant, even if no significant proper motion has been measured (see Figure **??**).

A stripped-giant companion would link the progenitor to the symbiotic single-degenerate channel (?) for which the symbiotic binaries TCrB and RS Oph are well studied candidates. Indeed, (?) argued that the ultracool low-mass helium white dwarfs (with masses $> 0.3\,M_\odot$) that have been identified in recent years are most likely the stripped-giant companions that survived SN Ia explosions, which could provide some further possible support for such a scenario for Tycho-G.

If the association is real, Tycho-G's displacement to the SE of the geometric center of the remnant as defined by radio and X-ray observations might be interpreted as being due to the remnant's interaction with an inhomogeneous ISM. Deep optical images of the remnant do show extended diffuse emission along the eastern and northeastern limbs interpreted as shock precursor emission (?). This along with an absence of detected Balmer-dominated optical emission along the whole of the western and southern limbs suggests a density gradient of the local interstellar medium with increasing density towards the NE. An east-west density gradient has also been inferred from detailed radio expansion rate measurements (?). Such an E–W density gradient could have led to a more rapid expansion toward the west giving rise to a small shift in the apparent geometric center away from the SE without creating a highly distorted remnant. However, there are problems with this explanation. Deviations from spherical symmetry in both radio and X-ray images of the remnant are relatively small (**??**), and the remnant is most extended along the eastern and northeastern limbs, just where one finds the greatest amount of extended diffuse optical emission. Moreover, the remnant's expansion rate appears lowest toward the northeast (PA = 70 degrees), not the southeast (?). Although the argument that Tycho-G's SE displacement from the remnant's current geometric center is a result of an asymmetrical expansion is not strong, it remains a possibility.

The most conclusive way of confirming a stripped-giant scenario for Tycho-G would be an independent, precise measurement of the distance to Tycho-G which in combination with measurements of the gravity and effective temperature would help to constrain Tycho-G's mass. Unfortunately, such a measurement will most likely have to wait for the advent of the GAIA satellite. Alternatively, one may be able to single out a stripped giant from a normal G2IV star through nucleosynthesis signatures, specifically evidence for CNO-processed material (or other nucleosynthetic anomalies). While a normal G2IV star is unlikely to show CNO-processed material at the surface, a stripped giant is likely to do so. Unfortunately, the data presented here are not of adequate quality to explore the detailed properties of Tycho-G's atmosphere.

2.7. Outlook and Future Observations

Presently, we believe the evidence for Tycho-G's association with the Tycho SN is interesting, but not conclusive. A possible scenario if Tycho-G is the donor star, would be that of a stripped giant scenario discussed in section 6. However, there are still other stars that have not been adequately scrutinized. **?** have found a star (RP04 Star-E) which may contain blueshifted Fe I lines, indicating their association with the remnant. Unfortunately, the star has neither a significant peculiar radial velocity (**?**; RP04) nor a significant peculiar proper motion (RP04 and confirmed by our work; see Table **??**).

High-resolution spectroscopy of each candidate in the remnant's center is necessary to precisely determine each star's physical parameters. However, the small observed velocities of the remaining stars suggest that the donor star would have needed to be a giant at the time of explosion. Using RP04's observed values, none of the stars in the remnant's center appear consistent with what is expected of a giant star as the donor star except possibly for Star-A. We also note that there is an additional star present in archived HST images, not cataloged in RP04, offset from RP04's star A by 0.5″ E and 0.2″ N at $m_V = 16.8$, $(B-V) = 1.0$. This star, near the remnant's centre, has a color consistent with an F-star (assuming that it is behind the bulk of the line of sight reddening), but it will require adaptive optics to obtain its spectrum given its proximity to the 13th magnitude Star-A. This star could potentially be a non-giant progenitor.

If future observations are unable to pinpoint a viable donor star, other progenitor scenarios will have to be considered. These include the double degenerate scenario, or a scenario where there is a long time delay between the accretion phase of a donor star onto the white dwarf, and the ultimate supernova explosion.

We would like to thank the Subaru HDS team for taking these observations in service mode. This paper makes use of data obtained from the Isaac Newton Group Archive which is maintained as part of the CASU Astronomical Data Centre at the Institute of Astronomy, Cambridge. This publication makes use of data products from the Two Micron All Sky Survey, which is a joint project of the University of Massachusetts and the Infrared Processing and Analysis Center/California Institute of Technology, funded by the National Aeronautics and Space Administration and the National Science Foundation. This work also makes use of POSS-I data. The National Geographic Society - Palomar Observatory Sky Atlas (POSS-I) was made by the California Institute of Technology with grants from the National Geographic Society. WEK, BPS and MA are supported by the Australian Research Council (grant numbers DP0559024, FF0561481). This paper was conceived as part of the Tokyo Think Tank collaboration, and was supported in part by the National Science Foundation under Grant No. PHY05-51164. This work was supported in part by World Premier International Research Center Initiative (WPI Program), MEXT, Japan, and by the Grant-in-Aid for Scientific Research of the Japan Society for the Promotion of Science (18104003, 18540231, 20540226) and MEXT (19047004, 20040004). Additionaly we would like to thank Pilar Ruiz Lapuente and her team for the valuable discussions we had in regards to the manuscript. We would also like to thank our referee, who provided us with a very detailed and thorough analysis of the first manuscript and subsequent revisions.

CHAPTER 3

SN1006

sdfsfdsfsdf

CHAPTER 4

AUTOMATIC FITTING OF OPTICAL TYPE IA SUPERNOVA SPECTRA - THE DALEK PROJECT

The last chapters (Chapters **??** were dedicated to the hunt for donor stars and did not use the measurements from the SN Ia-phenomenon itself. In this chapter we will describe the extraction of yields and energies from optical spectra.

The two main sources of information in spectra, are the spectra themselves as well as their time evolution. There have been a few attempts to extract the details of the stellar explosions from one or two of these sources. All of them employ the technique of fitting the spectra using synthetic spectra. One of the main parts is the radiative transfer program that creates the synthetic spectra. There are several different radiative transfer-codes in the community.

? wrote a very simple radiative transfer code called SYNOW. SYNOWis a highly parametrized code and thus is mainly used for line identification rather than actual fitting of supernova spectra. It runs The main code (henceforth ML MONTE CARLO) used in this work is an evolved code of **??**. Compared to the SYNOW-code the ML MONTE CARLO-code calculates a radiative equlibirum tepmerature and uses this to compute internally consistent ionization ratios. In addition ML MONTE CARLOtakes electron scattering into account as well as allowing for photon branching.

Codes such as PHOENIX**?**, SEDONA **?** and ARTIS **?** are powerful 3D radiative transfer codes. They are the most "physical" codes available but take hours on supercomputers to produce spectra. These codes, however, are not feasible for fitting observed spectra as they take too long for each iteration.

The main aim of this work was to automatically fit the torrent of observed spectra expected from the next generation of supernova searches. We opted to use the ML MONTE CARLO-code as it provides a good compromise between speed and "realism".

In section **??**we will introduce a the inner-workings of the ML MONTE CARLO-code. We will discuss the properties of the search space in **??** and will introduce our optimisation strategies in **??**. Finally we will conclude and give an outlook over future work for this unfinished project in section **??**.

4.1. The ML MONTE CARLO-Code

The supernova can be divided in two different phases: the photospheric phase and the nebular phase. The ML MONTE CARLO-code only models the photospheric phase. In this photospheric phase the supernova is treated like a sharp photosphere emitting a black-body spectrum with a fast moving layer of ejecta above that.

There are many physical processes in radiative transfer. Of those the Bound-free opacity has the biggest contribution to the final spectrum. In addition, Thompson scattering is thought to have an important effect in redistributing the flux. As ML MONTE CARLOis required to run fast only Bound-Free opacity as well as Thompson scattering is implemented in the code.

Unlike stellar atmospheres in supernova ejecta one needs to consider the photon's doppler shift in relation to the surrounding medium. One major assumption that the code makes is that of the Sobolev approximation. This means that at the interaction between photon and line resonance happens only at one specific point (thus disregarding any broadening effects to the line). For example a photon in free flight from the photosphere will be able to interact with resonance lines of lower and lower frequencies. The Sobolev approximation makes the code relatively fast

Another assumption that ML MONTE CARLOmakes is that the ejecta is in homologous expansion. This means that the velocity is a linear function of the radius:

$$v = r/t.$$

Combining both the Sobolev approximation with the assumption of homologous expansion yields this relatively simple formulat for line opacities:

$$\tau_{ul} = \frac{\pi e^2}{m_e c} f \lambda t_{\mathrm{exp}} n_l \left(1 - \frac{g_l n_u}{g_u n_l}\right),$$

where τ_{ul} denotes the opacity going from the u-state to the l-state, e is the electron charge, m_e is the electron mass, f is the oscilator strength of the line, λ denotes the wavelength, $t_e xp$ the time since explosion, n_x the number of atoms in the state x and g_x is the statistical weight of the state x. Both homologous expansion and Sobolev approximation have their caveats. In the case of homologous expansion it is thought to be a very good approximations after the first few minutes after the explosion. The main caveat for Sobolev approximation is that a line is not a delta-function, as assumed in the Sobolev approximation. If too strong bound-bound lines are close in frequency space it can lead to the first line shielding the second line. In summary for fast supernova fitting both approximations seem to still allow for a relatively well fitting spectrum.

We have discussed the propagation of the photons in the plasma but have not discussed the state of the plasma yet. The simplest assumption for the state one can make is local thermodynamic equilibrium. In this case the Boltzmann formula describes the level populations in a single ion:

$$\frac{n_j}{n_{\text{ground}}} = \frac{g_j}{g_{\text{ground}}} e^{-(\epsilon_j - \epsilon_{\text{ground}})/kT}$$

Similarly we can calculate the ionization state using the Saha-equation:

$$\frac{N_j}{N_{j+1}} = n_e \frac{U_j(T)}{U_{j+1}(T)} C_I T^{-3/2} e^{\chi/kT},$$

where U_j is the partition function and C_I is a constant. As the ionization likelyhood depends on the internal electronic state of the atom the partition function sums up over the different states:

$$U_j = \sum_i g_{i,j} e^{-\frac{E_{i,j}}{kT}},$$

where i describes the excitation states and j the ionization states. The other symbols have their usual meaning. The sum normally diverges slowly so one in practice just sums up until a highly excited state.

The ML MONTE CARLO uses the so called *nebular approximation* which will calculate the excitation and ionization state of the SNe at nearly LTE cost. In this nebular approximation they introduce a dilution factor W. This is a purely geometrical factor. Treating the photosphere as a point source the factor would result in $W = 1/r^2$ with r being the distance from the center. As the photosphere is expanded the dilution factor has a slightly more complex formula. An important point to note is that purely theoretical at the photosphere the dilution factor is 0.5.

The mean intensity for the supernova at a specific zone is given as:

$$J = WB(T_R),$$

where T_R is the radiative temperature. The radiative temperature is estimated in the ML MONTE CARLO by matching the mean frequency of $B(T_R)$ with the mean frequency of the photon packets in the current zone (Wien approximation). W is chosen so that the frequency-integrated intensity matches the photon distribution.

Using W and J one now can calculate the electronic and ionization states of the plasma:

$$\frac{n_j}{n_{\text{ground}}} = W \left(\frac{n_j}{n_{\text{ground}}} \right)_{T_R}^{\text{LTE}}$$

and

$$\frac{N_j}{N_{j+1} n_e} = W \left(\frac{N_j}{N_{j+1} n_e} \right)_{T_R}^{\text{LTE}}$$

In the simplest case we can treat the ejecta as homogeneous in temperature and abundance. For now we will also assume a pure scattering line interaction. This means that the photon is absorbed at a resonance frequency and then instantaneously reemitted with the same frequency into a random direction. This in in contrast to photon branching which we will discuss later.

We assume a time since explosion t_e, a photospheric velocity v_{ph}, $L_{\mathrm{bol}}$and an abundance distribution for the chosen elements. W7 (**?**) is used in the ML MONTE CARLO as a density structure.

The one dimensional model is divided into multiple zones that each have the same abundance but a different density. Using an initial guess of T_{eff} for the photosphere, one can calculate the plasma condition in each shell.

The Monte-Carlo simulation begins. A photon packet is emitted with a random frequency and a random angle drawn from a Blackbody distribution $B(T)$. Each photon packet contains the same energy (more photons per packet in the red than in the blue). An event optical depth is calculated from a uniform random distribution so that $\tau_{\mathrm{event}} = -ln(z); z \in (0, 1]$. In the next step there are three possible outcomes. We calculate the length of the path (s_e) that the packet can travel freely before τ_{event} is equal to the Thompson scattering opacity $\tau_{\mathrm{event}} = \sigma_{\mathrm{T}} n_e s_e$. Next we calculate the same path length for the lines s_l using as a target opacity $\tau_e + \tau_{\mathrm{line}}$. If both paths are longer than the path to exit the current zone, then the photon exits the current zone and a new Monte Carlo process begins. If however s_e is the shortest then Thompson scattering occurs and the photon is assigned a new direction and a new τ_{event} is drawn and the process begins anew.

In the case of line scattering the excited atom can de-excite through many lines. ML MONTE CARLOrandomly chooses a downward transition for the whole packet (taking the appropriate weights into account). The number of photons in the packet is adjusted to ensure that the energy is conserved in the comoving frame.

There are two possibilities for the final fate of the photon. Either it is reabsorbed into the photosphere or is emitted from the supernova.

When initializing the state of the plasma one assumes an initial guess for the photon temperature. The Monte-Carlo simulation is run and records each packet status at the midpoint of each shell. This information is used to calculate a new photospheric temperature and an updated plasma condition (level population and ionization). This procedure is repeated until the photospheric temperature converges. Once convergence is reached the actual Monte-Carlo simulation begins.

The final spectrum is not calculated using the escaping packets. Instead we calculate the optical depths using and then calculate the emerging spectrum using the formal integral. This has the advantage of reducing noise in the spectrum due to Monte-Carlo noise and gives very good results.

A more detailed description of the code can be found in **??**.

4.2. Manually fitting a Type Ia supernova

When fitting manually there are several features that help guide the direction of the fit. We will attempt to explain by using a spectrum of SN2002bo (cite?????) 10 days before maximum. In this section we will only talk about fits with no abundance stratification. Stephan Hachinger has kindly provided his manually obtained best fitting parameters (for the supernova at this stage (see Figure **??**). Directly measurable are the redshift of the supernova (and implied distance) and the time of the spectrum relative to maximum. We assume calculate the time since explosion assuming a rise time of 19.5 days. The other parameters are initialized using empirical data.

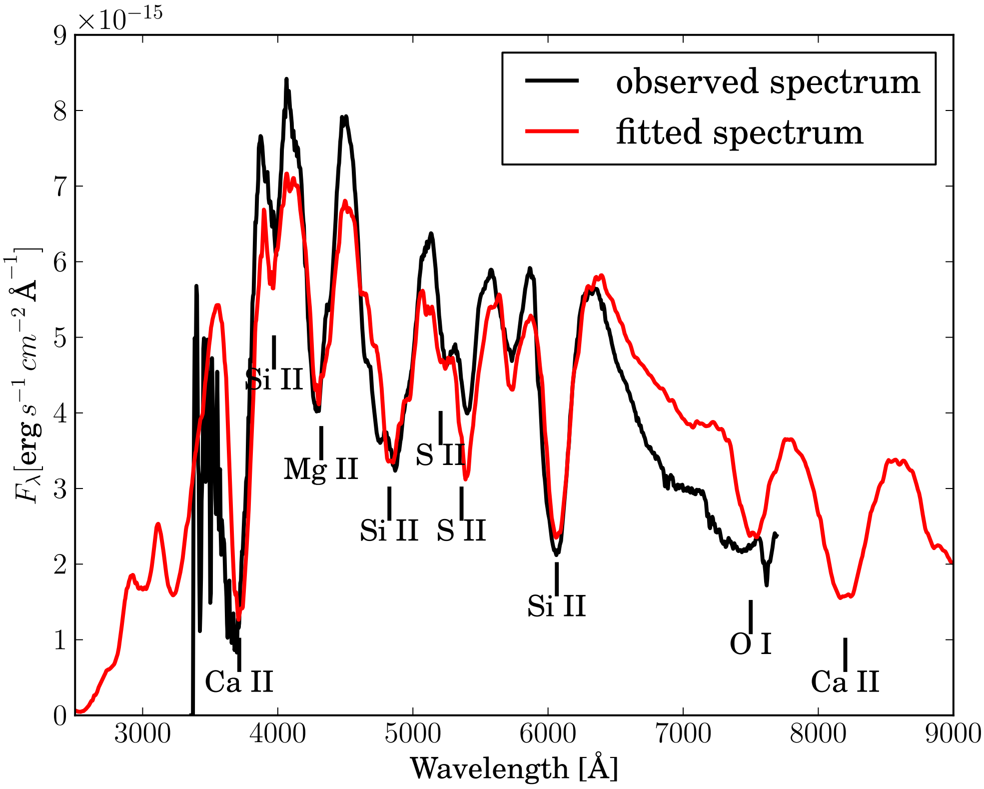

Figure 4.1 example caption

The chosen fundamental parameters are $\log L/L_\odot = xx$, $v_{\mathrm{ph}} = xxx$. We have listed the non-zero abundances in Table **??**.

The P-Cygni profiles of many features are easily visible. The Calcium line in the blue can be seen to be to blueshifted in relation to the model. This property is not unusual and is thought to come from high velocity component at the outer edge of the ejecta. The next major known discrepancy that can be seen is the excess of flux redwards of ≈ 6200Å. This is a region that usually does not fit well as the underlying black body spectrum overestimates the flux in this region. When fitting manually often one tries to fit the depth the lines instead of the continuum.

There are three main parameters that have the most influence on the overall fit: Luminosity, photospheric velocity and abundance in iron group elements.

A large offset in L to the best fit paramater is easily visible as a large offset of the continuum (see Figure **??**. Thus it is easy to constrain the parameter space in L initially. L also has influence on the temperature of the model through:

$$L_{\mathrm{bol}} = 4\pi\sigma R^2 T^4 = 4\pi\sigma\, v_{\mathrm{ph}}\, t_{\mathrm{exp}}.$$

Velocity in astronomy is often measured using the doppler shift. In this case however it is hard to measure the photospheric velocity as lines are created at different depths and thus at different velocities. This smears out the line profiles which makes fitting velocities nearly impossible using this technique. The main impact of photospheric velocity is establishing the temperature given a luminosity. A model with a too high photospheric velocity will have expanded more than the real spectrum at that time and will be cooler. This results in a spectrum that is too luminous in the red and not luminous enough in the blue (see Figure **??**). A secondary effect is that the ion population will be different to the actual supernova and the line spectrum differs.

Figure 4.2 example caption

The iron group element have a similar influence on the overall flux distribution as the photospheric velocity. As we assume no stable Cobalt and the input parameters for Nickel, Cobalt and Iron are ^{56}Ni56$_0$ and ^{56}Fe56$_0$ and calculate the abundances using radioactive decay. Ti and Cr have no easily identifiable single lines in the observed spectra, but provide line blanketing in the blue. We often lock their ratios and only use one abundance as an input parameter.

These elements cause photons to be absorbed in the UV and reemit in the red. A too high abundance will suppress the flux in the blue too much and will cause the spectrum to be over-luminous in the red (see Figure **??**). Although physically different from the photospheric velocity, phenomenologically these are similar. The degeneracy is broken by identifiable Fe-Lines in the red part of the spectrum as well as the ionization balance determined by the temperature (influenced by photospheric velocity). This near degeneracy causes a very complex search space.

There are six other abundances that are taken into account when fitting: Carbon, Oxygen, Magnesium, Silicon, Sulfur and Calcium. Among these Oxygen plays a special role. It does not have lines except the Oxygen triplet at 7778 Å. In our fitting routine it acts as a buffer element and is assigned the remaining fraction that is left after all elements have been given abundances.

The first element that is usually adjusted from its initial value is Calcium. The Calcium line is relatively easy to identify and

4.3. Genetic Algorithms

CHAPTER 5

CONCLUSION AND FUTURE WORK

CHAPTER 6

LINEAR INTERPOLATION IN N-DIMENSIONS

INTERPOLATION is one of the most common operations in astronomy. Irregardless if one needs to resample spectra on a different wavelength grid to co-add them, projecting images to align them or interpolating physical quantities in N-dimensional fluid dynamics simulation, interpolation plays a central role. Interpolation can be described as a special case of curve fitting which requires the function to go through all points.

In one dimension interpolation is relatively easy and there exist multiple methods. The simplest method is nearest-neighbour interpolation in which the interpolation picks the closest neighbour point to the point to be interpolated.

Linear interpolation is one of the most common methods of interpolation. The two neighbouring points of the point to be interpolated are found and using their slope and offset the value is interpolated.

There exist more complex interpolation methods like splines that employ polynomials of n-th degree whose first and second derivation need to be the same at the data points.

Where there exist many methods for interpolation in one dimensional space, the number of options decreases rapidly with the number of dimensions increasing. Although the number of viable options is decreasing there exist still a number of methods for n-dimensional interpolation. We will focus on the implementation of linear interpolation in N-dimensions, although there are other options like nearest neighbour interpolation and Radial basis function.

For our linear interpolation we have opted to use Delauney Triangulation as a interpolation method.

The interpolation using Delauney Triangulation employs multiple steps to arrive at an interpolation.

First a delauney triangulation is performed on the existing grid. As a next step we need to find the simplex that contains the point to be interpolated. Finally we will use the barycentric coordinate system of the simplex to perform the actual interpolation.

6.1. Delauney triangulation

A triangulation describes the process of connecting all points in a set with straight lines without any two lines crossing (see Figure **??**). It is obvious that there many ways for a set to to be triangulated. All triangulations however have the same outer boundary called the convex hull. One special kind of triangulation is the Delauney Triangulation. The Delauney Triangulation can be defined a various abstract ways and has intriguing properties.

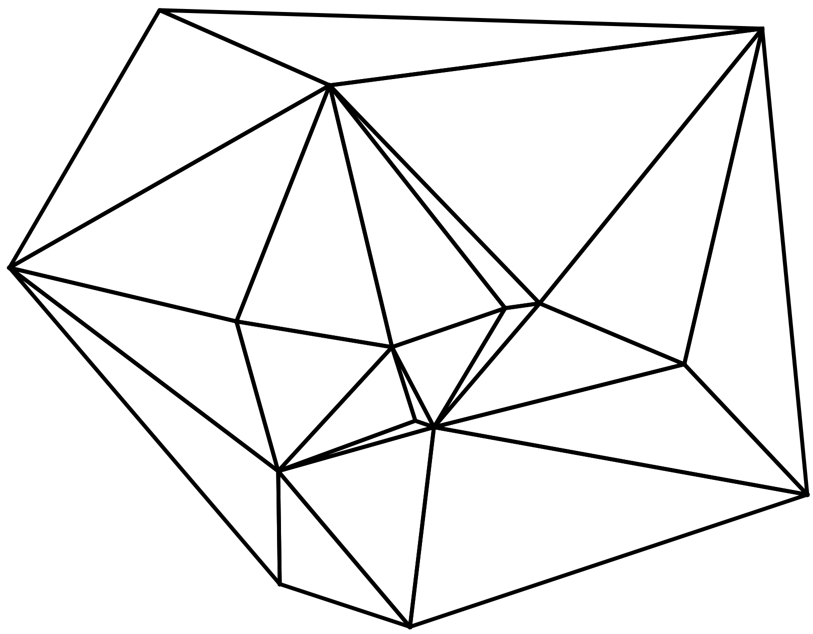

Figure 6.1 The delauney triangulation of 20 points is shown above

One such defintion is that the circum-circle of each triangle must only contain three points. Figure **??**, a simple two dimensional example, shows one *legal* triangulation and one *illegal* triangulation. One can see in the *illegal* triangulation that the circum-circles of both triangles contain more than tree points. By doing a simple "*edge-flip*" one arrives at the delauney triangulation. In addition this ensures that the triangulation gives the largest minimum angle for both triangles. There

Delauney Triangulation and convex hulls have a very interesting relation. It is possible construct the Delauney Triangulation in n dimensions from a convex hull of the points projected on paraboloid in n+1 dimensions. Figure **??** shows an example of a Delauney Triangulation in two dimensions constructed from the convex hull in three dimensions. To project the points onto the paraboloid one just square sums the coordinates n dimensions and uses this as the coordinate for the point in n+1 dimensions.

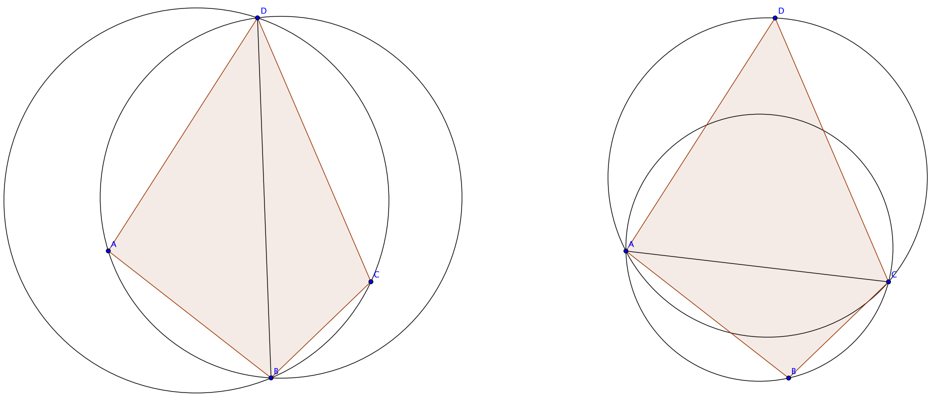

Figure 6.2 The left figure shows an "*illegal*" triangulation of the 4 points. Both circles include all the points. With a so called edge flip one can arrive at a "*legal*" triangulation

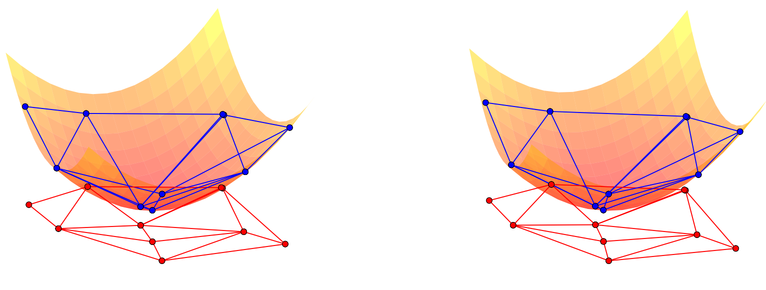

Figure 6.3 Stereogram (**?**) of the projection of the convex hull in three dimensions to form the delauney triangulation in two dimensions

6.2. Convex Hull

In section **??** we have described the relation between the convex hull and the Delauney Triangulation. There are multiple ways to construct the convex hull for N points, we will limit ourselves to the description of the Quickhull algorithm. Similar to the Quicksort algorithm it follows the divide and conquer method.

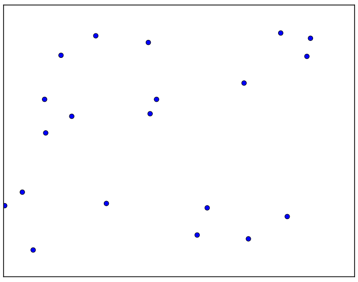

(a) Twenty points for which we are trying to find the convex hull

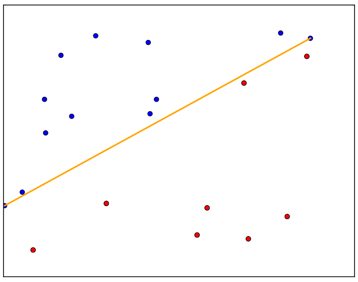

(b) We find the points with the lowest and highest x-value and connect them with a line

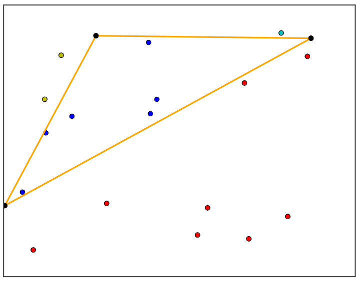

(c) Continuing with the points on the left (same process happens recursively on the right) we find the point furthest away from the line. We then draw two more lines and build a triangle. The points inside of the triangle are not part of the convex hull and are discarded. We will repeat the current step with the two new lines of the triangle.

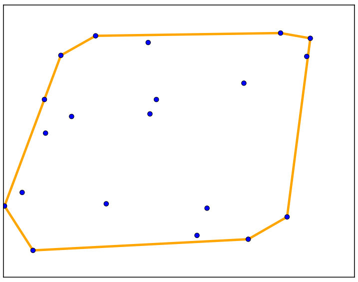

(d) We have found points of the convex hull once we can't build a new triangle anymore.

Figure 6.4 Building of a convex hull.

As an initial input we have N data points. Although this method works in n-dimensions, we will show an example in two dimensions. The first operation is finding the two extreme points in the horizontal axis, which are guaranteed to be part of the convex hull. We connect these two extreme points thus creating a division between the left and right point set. Now the divide and conquer method begins. We will only describe what happens to the left side, but imply that the same steps are taken on the right side. We find the point furthest away from the dividing line and add it. This forms a triangle with all points inside the triangle not belonging to the convex hull and thus we exclude them. The triangle again divides the remaining points into two sets, one left of the triangle and one right which are again iterated over recursively.

The method is repeated until each subset only contains the start and end point of the dividing line. We have created the convex hull, which if projected to a $d-1$-dimensional space provides the Delauney Triangulation of the projected points.

6.3. Barycentric coordinates system

The actual interpolation transforms the interpolant's coordinate into the barycentric coordinates of the containing triangle.

One can construct the barycenter of a triangle by drawing lines from each point to the midpoint of the opposing side (see Figure **??**).

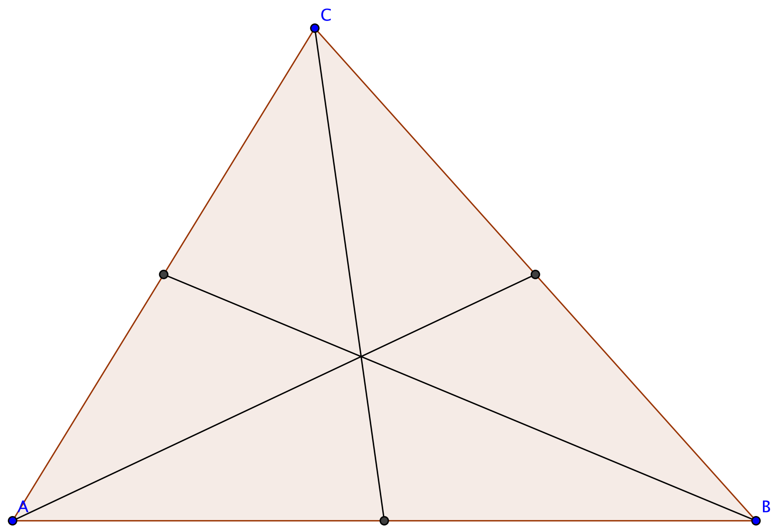

Figure 6.5 The triangle and its barycenter marked by the intersection of lines.

The coordinates of the barycenter M can simply be expressed by,

$$\vec{M} = \frac{1}{3}(\vec{A} + \vec{B} + \vec{C}).$$

Not only the barycenter can be expressed by the vectors of $\vec{A}$, $\vec{B}$ and $\vec{C}$ but every point p inside the triangle can be expressed by,

$$\vec{p} = \alpha\vec{A} + \beta\vec{B} + \gamma\vec{C},$$

where,

$$\alpha + \beta + \gamma = 1$$

. α, β and γ are called the barycentric coordinates. If the point p lies within the triangle all barycentric coordinates are positive.

6.4. Triangle Finding and Interpolation

To calculate the interpolation using barycentric coordinates we need to find the triangle that contains the interpolant. We use a method called directed walk (priv. comm. Pauli

Virtanen). We choose a random starting triangle and calculate the barycentric coordinates for the interpolant and test if they are larger than 0. If all of them are larger than 0 we have found the containing Triangle. If the n-th (0,1 or 2 for two dimensions) barycentric coordinate is negative we jump to the neighbouring triangle which is opposite the n-th point. This is iterated until the containing triangle is found or the next jump would lead outside the convex hull. For the latter the point is outside of grid and can not be interpolated.

Once we find the triangle that contains the point p and we know the barycentric coordinates we can simply interpolate the function at the point by,

$$f(\vec{p}) = \alpha f(\vec{A}) + \beta f(\vec{B}) + \gamma f(\vec{C})$$

where $\vec{A}$, $\vec{B}$ and $\vec{C}$ are the points of the triangle.

6.5. Conclusion

We have described the method of linear interpolation using delauney triangulation in two dimensions, but the method is extensible to N-dimensions. The triangles (3-simplex) become n-simplices in n-dimensions (e.g. Tetrahedron in 3 dimensions). The method, however, is very similar for higher dimensions.

In this work we have made extensive use of n-dimensional linear interpolation using the implementation present in scipy (**?**)(using the LinearNDInterpolator function). In this case creation of the convex-hull is performed by the QHULL implementation described in **?**.

We have tested the performance of the algorithm by creating a three dimensional grid with $20 \times 10 \times 10$ gridpoints and an array of 10, 000 double values at each gridpoint. On a standard 2011 MacBook Pro we have measured the initial build of the interpolation grid to 256 ms . The interpolation for random points took on average 601 μ s. This technique lends it very well to explore large datasets even on moderately equipped machines.

There are drawbacks however. We have used this technique extensively to interpolate a spectral grid in three dimension (T_{eff}, $\log g$ and [Fe/H]). When trying to extract stellar parameters from an input spectrum we calculated the χ^2 for the observed spectrum against the grid. The non-differentiability at the ridges can be seen even in the χ^2 space. Optimizers that employ gradient methods (such as MIGRAD **?**) show difficulties in some regions of the search space.

In summary, the presented linear n-dimensional interpolator is a very robust and quick way to explore large parameter spaces without having to compute each single point.

Future work will be directed to exploring other n-dimensional interpolators in the astrophysical context.

BIBLIOGRAPHY

Aller, L. H., Appenzeller, I., Baschek, B., Duerbeck, H. W., Herczeg, T., Lamla, E., Meyer-Hofmeister, E., Schmidt-Kaler, T., Scholz, M., Seggewiss, W., Seitter, W. C., & Weidemann, V. 1982, Landolt-Börnstein: Numerical Data and Functional Relationships in Science and Technology (Berlin: Springer)

Altavilla, G., Fiorentino, G., Marconi, M., Musella, I., Cappellaro, E., Barbon, R., Benetti, S., Pastorello, A., Riello, M., Turatto, M., & Zampieri, L. 2004, MNRAS, 349, 1344

Arnett, W. D. 1969, Ap&SS, 5, 180

Baade, W. & Zwicky, F. 1934, Proceedings of the National Academy of Science, 20, 254

Barber, C. B., Dobkin, D. P., & Huhdanpaa, H. 1996, ACM TRANSACTIONS ON MATHEMATICAL SOFTWARE, 22, 469

Barbon, R., Ciatti, F., & Rosino, L. 1979, A&A, 72, 287

Baron, E., Bethe, H. A., Brown, G. E., Cooperstein, J., & Kahana, S. 1987, Physical Review Letters, 59, 736

Baron, E., Cooperstein, J., & Kahana, S. 1985, Physical Review Letters, 55, 126

Benetti, S., Cappellaro, E., Mazzali, P. A., Turatto, M., Altavilla, G., Bufano, F., Elias-Rosa, N., Kotak, R., Pignata, G., Salvo, M., & Stanishev, V. 2005, ApJ, 623, 1011

Bessell, M. S., Castelli, F., & Plez, B. 1998, A&A, 333, 231

Bildsten, L., Shen, K. J., Weinberg, N. N., & Nelemans, G. 2007, ApJ, 662, L95

Caccin, B., Cavallini, F., Ceppatelli, G., Righini, A., & Sambuco, A. M. 1985, A&A, 149, 357

Canal, R., Méndez, J., & Ruiz-Lapuente, P. 2001, ApJ, 550, L53

Cannon, R., Hambly, N., & Zacharias, N. Astronomical Society of the Pacific Conference Series, Vol. 232, , The New Era of Wide Field Astronomy, ed. R. ClowesA. Adamson & G. Bromage, 311–+

Cardelli, J. A., Clayton, G. C., & Mathis, J. S. 1989, ApJ, 345, 245

Cassam-Chenaï, G., Hughes, J. P., Ballet, J., & Decourchelle, A. 2007, ApJ, 665, 315

Chandrasekhar, S. 1931, ApJ, 74, 81

della Valle, M. & Livio, M. 1994, ApJ, 423, L31

Della Valle, M. & Panagia, N. 2003, ApJ, 587, L71

Eggleton, P. P. 1983, ApJ, 268, 368

Ensman, L. & Burrows, A. 1992, ApJ, 393, 742

Filippenko, A. V., Li, W. D., Treffers, R. R., & Modjaz, M. 2001, in Astronomical Society of the Pacific Conference Series, Vol. 246, IAU Colloq. 183: Small Telescope Astronomy on Global Scales, ed. B. Paczynski, W.-P. Chen, & C. Lemme, 121–+

Fink, M., Röpke, F. K., Hillebrandt, W., Seitenzahl, I. R., Sim, S. A., & Kromer, M. 2010, A&A, 514, A53+

Fisher, A. K. 2000, PhD thesis, THE UNIVERSITY OF OKLAHOMA

Garavini, G., Nobili, S., Taubenberger, S., Pastorello, A., Elias-Rosa, N., Stanishev, V., Blanc, G., Benetti, S., Goobar, A., Mazzali, P. A., Sanchez, S. F., Salvo, M., Schmidt, B. P., & Hillebrandt, W. 2007, A&A, 471, 527

Gaskell, C. M., Cappellaro, E., Dinerstein, H. L., Garnett, D. R., Harkness, R. P., & Wheeler, J. C. 1986, ApJ, 306, L77

Gerardy, C. L., Höflich, P., Fesen, R. A., Marion, G. H., Nomoto, K., Quimby, R., Schaefer, B. E., Wang, L., & Wheeler, J. C. 2004, ApJ, 607, 391

Ghavamian, P., Raymond, J., Hartigan, P., & Blair, W. P. 2000, ApJ, 535, 266

Gilfanov, M. & Bogdán, Á. 2010, Nature, 463, 924

Gooch, R. in , Astronomical Society of the Pacific Conference Series, Vol. 101, Astronomical Data Analysis Software and Systems V, ed. G. H. JacobyJ. Barnes, 80–+

Gutiérrez, J., Canal, R., & García-Berro, E. 2005, A&A, 435, 231

Guy, J., Astier, P., Baumont, S., Hardin, D., Pain, R., Regnault, N., Basa, S., Carlberg, R. G., Conley, A., Fabbro, S., Fouchez, D., Hook, I. M., Howell, D. A., Perrett, K., Pritchet, C. J., Rich, J., Sullivan, M., Antilogus, P., Aubourg, E., Bazin, G., Bronder, J., Filiol, M., Palanque-Delabrouille, N., Ripoche, P., & Ruhlmann-Kleider, V. 2007, A&A, 466, 11

Hachisu, I., Kato, M., & Nomoto, K. 1996, ApJ, 470, L97 [LINK]

Hachisu, I., Kato, M., & Nomoto, K. 1999b, ApJ, 522, 487

Hachisu, I., Kato, M., Nomoto, K., & Umeda, H. 1999a, ApJ, 519, 314 [LINK]

Hamilton, A. J. S. & Fesen, R. A. 1988, ApJ, 327, 178 [LINK]

Han, Z. 2008, accepted for publication in ApJL [LINK]

Han, Z. & Podsiadlowski, P. 2004, MNRAS, 350, 1301 [LINK]

Harkness, R. P., Wheeler, J. C., Margon, B., Downes, R. A., Kirshner, R. P., Uomoto, A., Barker, E. S., Cochran, A. L., Dinerstein, H. L., Garnett, D. R., & Levreault, R. M. 1987, ApJ, 317, 355

Hartwig, E. 1885, Astronomische Nachrichten, 112, 360

Hatano, K., Branch, D., Fisher, A., Baron, E., & Filippenko, A. V. 1999, ApJ, 525, 881

Hauschildt, P. H. & Baron, E. 1999, Journal of Computational and Applied Mathematics, 109, 41

Hernandez, J. I. G., Ruiz-Lapuente, P., Filippenko, A. V., Foley, R. J., Gal-Yam, A., & Simon, J. D. 2009, ApJ, 691, 1

Hillebrandt, W. & Niemeyer, J. C. 2000, ARA&A, 38, 191

Hirashita, H., Buat, V., & Inoue, A. K. 2003, A&A, 410, 83

Howell, D. A. 2001, ApJ, 554, L193

Iben, I. J. NATO ASIC Proc. 486: Thermonuclear Supernovae, ed. , P. Ruiz-LapuenteR. Canal & J. Isern (Dordrecht: Kluwer), 111

Ihara, Y., Ozaki, J., Doi, M., Shigeyama, T., Kashikawa, N., Komiyama, K., & Hattori, T. 2007, PASJ, 59, 811

Iliadis, C. 2007, Nuclear Physics of Stars, ed. Iliadis, C. (Wiley-VCH Verlag)

James, F. & Roos, M. 1975, Comput. Phys. Commun., 10, 343

Jha, S., Riess, A. G., & Kirshner, R. P. 2007, ApJ, 659, 122

Justham, S., Wolf, C., Podsiadlowski, P., & Han, Z. 2008, submitted

—. 2009, A&A, 493, 1081

Kasen, D. 2006, ApJ, 649, 939

Kasen, D., Röpke, F. K., & Woosley, S. E. 2009, Nature, 460, 869

Kasen, D., Thomas, R. C., & Nugent, P. 2006, ApJ, 651, 366

Kepler, S. O., Kleinman, S. J., Nitta, A., Koester, D., Castanheira, B. G., Giovannini, O., Costa, A. F. M., & Althaus, L. 2007, MNRAS, 375, 1315

Kerzendorf, W. E., Schmidt, B. P., Asplund, M., Nomoto, K., Podsiadlowski, P., Frebel, A., Fesen, R. A., & Yong, D. 2009, ApJ, 701, 1665

Kirshner, R. P. & Kwan, J. 1974, ApJ, 193, 27

Krause, O., Tanaka, M., Usuda, T., Hattori, T., Goto, M., Birkmann, S., & Nomoto, K. 2008, Nature, 456, 617

Kromer, M. & Sim, S. A. 2009, MNRAS, 398, 1809

Leonard, D. C. 2007, ApJ, 670, 1275

Lesaffre, P., Podsiadlowski, P., & Tout, C. A. 2005, Nuclear Physics A, 758, 463

Li, X.-D. & van den Heuvel, E. P. J. 1997, A&A, 322, L9 [LINK]

Mannucci, F., Della Valle, M., Panagia, N., Cappellaro, E., Cresci, G., Maiolino, R., Petrosian, A., & Turatto, M. 2005, A&A, 433, 807

Marietta, E., Burrows, A., & Fryxell, B. 2000, ApJS, 128, 615

Mazzali, P. A. 2000, A&A, 363, 705

Mazzali, P. A., Benetti, S., Altavilla, G., Blanc, G., Cappellaro, E., Elias-Rosa, N., Garavini, G., Goobar, A., Harutyunyan, A., Kotak, R., Leibundgut, B., Lundqvist, P., Mattila, S., Mendez, J., Nobili, S., Pain, R., Pastorello, A., Patat, F., Pignata, G., Podsiadlowski, P., Ruiz-Lapuente, P., Salvo, M., Schmidt, B. P., Sollerman, J., Stanishev, V., Stehle, M., Tout, C., Turatto, M., & Hillebrandt, W. 2005, ApJ, 623, L37

Mazzali, P. A. & Lucy, L. B. 1993, A&A, 279, 447

Meikle, W. P. S. 2000, MNRAS, 314, 782

Mennekens, N., Vanbeveren, D., De Greve, J. P., & De Donder, E. 2010, A&A, 515, A89+

Minkowski, R. 1941, PASP, 53, 224

Mohamed, S. & Podsiadlowski, P. 2011, in Asymmetric Planetary Nebulae 5 Conference

Noguchi, K., Ando, H., Izumiura, H., Kawanomoto, S., Tanaka, W., & Aoki, W. 1998, in Proc. SPIE, Optical Astronomical Instrumentation, ed. S. D'Odorico, Vol. 3355, 354

Nomoto, K. 1982, ApJ, 253, 798 [LINK]

Nomoto, K. & Iben, Jr., I. 1985, ApJ, 297, 531

Nomoto, K. & Kondo, Y. 1991, ApJ, 367, L19

Nomoto, K., Saio, H., Kato, M., & Hachisu, I. 2007, ApJ, 663, 1269 [LINK]

Nugent, P., Phillips, M., Baron, E., Branch, D., & Hauschildt, P. 1995, ApJ, 455, L147+

Nugent, P., Sullivan, M., Ellis, R., Gal-Yam, A., Leonard, D. C., Howell, D. A., Astier, P., Carlberg, R. G., Conley, A., Fabbro, S., Fouchez, D., Neill, J. D., Pain, R., Perrett, K., Pritchet, C. J., & Regnault, N. 2006, ApJ, 645, 841

Ozaki, J. & Shigeyama, T. 2006, ApJ, 644, 954 [LINK]

Pakmor, R., Kromer, M., Röpke, F. K., Sim, S. A., Ruiter, A. J., & Hillebrandt, W. 2010, Nature, 463, 61

Pakmor, R., Röpke, F. K., Weiss, A., & Hillebrandt, W. 2008, A&A, 489, 943

Panagia, N., Van Dyk, S. D., Weiler, K. W., Sramek, R. A., Stockdale, C. J., & Murata, K. P. 2006, ApJ, 646, 369

Patat, F., Chandra, P., Chevalier, R., Justham, S., Podsiadlowski, P., Wolf, C., Gal-Yam, A., Pasquini, L., Crawford, I. A., Mazzali, P. A., Pauldrach, A. W. A., Nomoto, K., Benetti, S., Cappellaro, E., Elias-Rosa, N., Hillebrandt, W., Leonard, D. C., Pastorello, A., Renzini, A., Sabbadin, F., Simon, J. D., & Turatto, M. 2007, Science, 317, 924

Perlmutter, S., Aldering, G., Goldhaber, G., Knop, R. A., Nugent, P., Castro, P. G., Deustua, S., Fabbro, S., Goobar, A., Groom, D. E., Hook, I. M., Kim, A. G., Kim, M. Y., Lee, J. C., Nunes, N. J., Pain, R., Pennypacker, C. R., Quimby, R., Lidman, C., Ellis, R. S., Irwin, M., McMahon, R. G., Ruiz-Lapuente, P., Walton, N., Schaefer, B., Boyle, B. J., Filippenko, A. V., Matheson, T., Fruchter, A. S., Panagia, N., Newberg, H. J. M., Couch, W. J., & The Supernova Cosmology Project. 1999, ApJ, 517, 565

Phillips, M. M. 1993, ApJ, 413, L105

Phillips, M. M., Wells, L. A., Suntzeff, N. B., Hamuy, M., Leibundgut, B., Kirshner, R. P., & Foltz, C. B. 1992, AJ, 103, 1632

Podsiadlowski, P. 2003

Quimby, R., Höflich, P., Kannappan, S. J., Rykoff, E., Rujopakarn, W., Akerlof, C. W., Gerardy, C. L., & Wheeler, J. C. 2006, ApJ, 636, 400

Reynoso, E. M., Moffett, D. A., Goss, W. M., Dubner, G. M., Dickel, J. R., Reynolds, S. P., & Giacani, E. B. 1997, ApJ, 491, 816

Riess, A. G., Filippenko, A. V., Challis, P., Clocchiatti, A., Diercks, A., Garnavich, P. M., Gilliland, R. L., Hogan, C. J., Jha, S., Kirshner, R. P., Leibundgut, B., Phillips, M. M., Reiss, D., Schmidt, B. P., Schommer, R. A., Smith, R. C., Spyromilio, J., Stubbs, C., Suntzeff, N. B., & Tonry, J. 1998, AJ, 116, 1009

Riess, A. G., Filippenko, A. V., Li, W., Treffers, R. R., Schmidt, B. P., Qiu, Y., Hu, J., Armstrong, M., Faranda, C., Thouvenot, E., & Buil, C. 1999, AJ, 118, 2675

Riess, A. G., Press, W. H., & Kirshner, R. P. 1995, ApJ, 438, L17

Robin, A. C., Reylé, C., Derrière, S., & Picaud, S. 2003, A&A, 409, 523

Röpke, F. K. & Hillebrandt, W. 2005, A&A, 431, 635

Ruiter, A. J., Belczynski, K., & Fryer, C. 2009, ApJ, 699, 2026

Ruiz-Lapuente, P. 2004, ApJ, 612, 357

Ruiz-Lapuente, P., Burkert, A., & Canal, R. 1995, ApJ, 447, L69+

Ruiz-Lapuente, P., Comeron, F., Méndez, J., Canal, R., Smartt, S. J., Filippenko, A. V., Kurucz, R. L., Chornock, R., Foley, R. J., Stanishev, V., & Ibata, R. 2004, Nature, 431, 1069

Saio, H. & Nomoto, K. 1985, A&A, 150, L21

Schlegel, E. M. 1990, MNRAS, 244, 269

Schweizer, F. & Middleditch, J. 1980, ApJ, 241, 1039

Sim, S. A., Röpke, F. K., Hillebrandt, W., Kromer, M., Pakmor, R., Fink, M., Ruiter, A. J., & Seitenzahl, I. R. 2010, ApJ, 714, L52

Skrutskie, M. F., Cutri, R. M., Stiening, R., Weinberg, M. D., Schneider, S., Carpenter, J. M., Beichman, C., Capps, R., Chester, T., et al. 2006, ApJ, 131, 1163

Sneden, C. 1973, ApJ, 184, 839

Soderberg, A. M., Berger, E., Page, K. L., Schady, P., Parrent, J., Pooley, D., Wang, X.-Y., Ofek, E. O., Cucchiara, A., Rau, A., Waxman, E., Simon, J. D., Bock, D. C.-J., Milne, P. A., Page, M. J., Barentine, J. C., Barthelmy, S. D., Beardmore, A. P., Bietenholz, M. F., Brown, P., Burrows, A., Burrows, D. N., Byrngelson, G., Cenko, S. B., Chandra, P., Cummings, J. R., Fox, D. B., Gal-Yam, A., Gehrels, N., Immler, S., Kasliwal, M., Kong, A. K. H., Krimm, H. A., Kulkarni, S. R., Maccarone, T. J., Mészáros, P., Nakar, E., O'Brien, P. T., Overzier, R. A., de Pasquale, M., Racusin, J., Rea, N., & York, D. G. 2008, Nature, 453, 469

Tammann, G. A., Loeffler, W., & Schroeder, A. 1994, ApJS, 92, 487

Tanaka, M., Mazzali, P. A., Maeda, K., & Nomoto, K. 2006, ApJ, 645, 470

Tanaka, M., Mazzali, P. A., Stanishev, V., Maurer, I., Kerzendorf, W. E., & Nomoto, K. 2011, MNRAS, 410, 1725

Thomas, R. C., Branch, D., Baron, E., Nomoto, K., Li, W., & Filippenko, A. V. 2004, ApJ, 601, 1019

Turatto, M. 2003, in Lecture Notes in Physics, Berlin Springer Verlag, Vol. 598, Supernovae and Gamma-Ray Bursters, ed. K. Weiler, 21–36

Turatto, M., Benetti, S., & Pastorello, A. 2007, in American Institute of Physics Conference Series, Vol. 937, Supernova 1987A: 20 Years After: Supernovae and Gamma-Ray Bursters, ed. S. Immler, K. Weiler, & R. McCray, 187–197

van den Bergh, S. & Tammann, G. A. 1991, ARA&A, 29, 363

van Dyk, S. D., Treffers, R. R., Richmond, M. W., Filippenko, A. V., & Paik, Y. 1994, in Bulletin of the American Astronomical Society, Vol. 26, American Astronomical Society Meeting Abstracts, 1444–+

Vogt, F. & Wagner, A. 2011, Astrophysics and Space Science, submitted.

Weaver, T. A., Zimmerman, G. B., & Woosley, S. E. 1978, ApJ, 225, 1021

Webbink, R. F. 1984, ApJ, 277, 355

Wehrse, R. 1974, A list of all Fraunhofer lines of the Rowland tables arranged by elements (Heidelberg: Universität)

Whelan, J. & Iben, Jr., I. 1973, ApJ, 186, 1007

Winkler, P. F., Gupta, G., & Long, K. S. 2003, ApJ, 585, 324

Wood-Vasey, W. M., Friedman, A. S., Bloom, J. S., Hicken, M., Modjaz, M., Kirshner, R. P., Starr, D. L., Blake, C. H., Falco, E. E., Szentgyorgyi, A. H., Challis, P., Blondin, S., Mandel, K. S., & Rest, A. 2008, ApJ, 689, 377

Woosley, S. E., Heger, A., & Weaver, T. A. 2002, Reviews of Modern Physics, 74, 1015

Zhao, F., Strom, R. G., & Jiang, S. 2006, Chinese J. Astron. Astrophys., 6, 635

Zwicky, F. 1938, ApJ, 88, 529

Appendices

Long Boring Tables